# Manuscript Details

| | |
|---|---|
| **Manuscript number** | PALAEO_2017_139 |
| **Title** | Phosphatized early Cambrian archaeocyaths and small shelly fossils (SSFs) of southwestern Mongolia |
| **Article type** | Research Paper |


**Abstract**

Archaeocyaths are an enigmatic group of calcifying sponges prevalent in early Cambrian (Terreneuvian to Series 2) successions around the world and preserved predominantly in reefal buildups, but also in adjacent reworked deposits. Here we report exceptionally preserved phosphatized archaeocyaths and small shelly fossils from phosphatized reef flank deposits at the top of the Salaagol Formation of southwestern Mongolia. Recent chemostratigraphic age models suggest that these archaeocyaths are among the earliest reported in the Terreneuvian Stage 2 (Tommotian). These fossils provide a window into the mechanisms of archaeocyath phosphatization, a generally rare mode of archaeocyath preservation. To assess the composition and nature of phosphatization, fossil assemblages were examined in insoluble residue and thin section. These archaeocyaths are preserved as phosphatic internal molds in residue, and both phosphatized and unphosphatized archaeocyaths are present in thin section. The occurrence of internal molds and complementary mineralogical data suggest that the decay of organic material within the archaeocyaths created the necessary redox conditions for apatite nucleation. We propose that, shortly after death, this assemblage was transported to a deeper water environment, and that the presence of organic matter in a low oxygen setting led to abundant phosphatization of archaeocyaths.



| | |
|---|---|
| **Keywords** | phosphatization; taphonomy; Tommotian; Salaagol; Terreneuvian |



| | |
|---|---|
| **Corresponding Author** | Sara B Pruss |
| **Order of Authors** | Sara B Pruss, Camille Dwyer, Emily Smith, Francis Macdonald, Nicholas Tosca |


| | |
|---|---|
| **Suggested reviewers** | Stephen Dornbos, Paul Myrow, Susannah Porter, Stephen Rowland, S Xiao |

# Phosphatized early Cambrian archaeocyaths and small shelly fossils (SSFs) of southwestern Mongolia

Sara B. Pruss[a], Camille H. Dwyer[b], Emily F. Smith[c,d], Francis A. Macdonald[ed], and Nicholas J. Tosca[fe]

[a, *]Smith College, Department of Geosciences, Northampton, Massachusetts, 01063, USA

[b]Department of Earth and Planetary Sciences, University of New Mexico, Albuquerque, NM, 87131, USA

[c]Department of Paleobiology, Smithsonian Institution, Washington, DC 20013-7012, USA

[d]Department of Earth and Planetary Sciences, Johns Hopkins University, Baltimore, Maryland, 21218, USA

[ed]Department of Earth and Planetary Sciences, Harvard University, Cambridge, Massachusetts, 02139, USA

[fe]Department of Earth Sciences, Oxford University, Oxford, OX1 3AN, UK

[*]Corresponding author. Tel.: +1 413 585 3948
*Email Address:* spruss@smith.edu

## ABSTRACT

**Archaeocyaths are an enigmatic group of calcifying sponges prevalent in early Cambrian (Terreneuvian to Series 2) successions around the world and preserved predominantly in reefal buildups, but also in adjacent reworked deposits. Here we report exceptionally preserved phosphatized archaeocyaths and small shelly fossils from phosphatized reef flank deposits at the top of the Salaagol Formation of southwestern Mongolia. Recent chemostratigraphic age models suggest that these archaeocyaths are among the earliest reported in the Terreneuvian Stage 2 (Tommotian). These fossils provide a window into the mechanisms of archaeocyath phosphatization, a generally rare mode of archaeocyath preservation. ~~, and chemostratigraphic age models suggest that these archaeocyaths are among the earliest reported in the Terreneuvian Stage 2 (Tommotian).~~ To assess the composition and nature of phosphatization, fossil assemblages were examined in insoluble residue and thin section. These archaeocyaths are preserved as phosphatic internal molds in residue, and both phosphatized and unphosphatized archaeocyaths are present in thin section. The occurrence of internal molds and complementary mineralogical data suggest that the decay of organic material within the archaeocyaths created the necessary redox conditions for apatite nucleation. We propose that, shortly after death, this assemblage was transported to a deeper water environment, and that the presence of organic matter in a low oxygen setting led to abundant phosphatization of archaeocyaths.**



*Keywords: phosphatization, taphonomy, Tommotian, Salaagol, Terreneuvian*

## 1. Introduction

Before the Phanerozoic Eon, microbial and abiotic fabrics formed the main components of carbonate reefs (e.g., Grotzinger and James, 2000). During the Cambrian Period, archaeocyaths appeared as the first animals to secrete thick carbonate skeletons and occasionally operated as the framework of reefs (e.g., Debrenne and Vacelet, 1984; Rowland and Gangloff, 1988; Zhuravlev, 1989; Kruse, 1990; Wood, 1990; Wood et al., 1992). Archaeocyaths are typically difficult to extract from a limestone matrix because they have skeletons composed of calcite, which has generally limited the study of their internal structures to thin section analysis (Rigby and Gangloff, 1987). A few occurrences of phosphatized archaeocyaths have been found in Siberia (Dzik, 1994), Greenland (Skovsted, 2006), Antarctica (Myrow et al., 2002; Wrona, 2004;), China (Wang et al., 2010; Wang et al., 2012; Zhang et al., 2016), and Mongolia (Esakova and Zhegallo,1996; Smith et al., 2016, but the taphonomy and preservation of these fossils have not been described in detail. In general, the early diagenetic phosphatization of skeletal and soft-bodied organisms has led to exceptional preservation of morphologies and micrometer-scale skeletal textures, particularly during the later Ediacaran and Cambrian periods (Cook, 1992; Bengtson and Yue, 1997; Xiao and Knoll, 2000; Butterfield, 2003; Porter, 2004; Creveling et al., 2014b). Here, we examine the nature of preservation of phosphatized archaeocyaths in an unusual deposit in the Salaagol Formation of Mongolia to better understand the environment that led to the development of this taphonomic window.

Until very recently, the early Cambrian Salaagol Formation in the Zavkhan Terrane of southwestern Mongolia had only been studied at two localities: Salaa Gorge and the Zuun-Arts Ridge (Brasier et al., 1996; Kruse et al., 1996). Calcareous archaeocyaths were examined and identified at the species level in thin section, and the reef morphology was described at the outcrop level (Wood et al., 1993; Kruse et al., 1996). More recently, during a detailed basin-wide study of the Terreneuvian and Series 2 Cambrian strata on the Zavkhan Terrane, archaeocyaths were identified at several additional localities, and phosphatized archaeocyaths and small shelly fossils (SSFs) were discovered in the uppermost beds of the Salaagol Formation, at the contact with the overlying Khairkhan Formation (Smith et al., ~~2015~~2016). These fossils are preserved in a series of laterally discontinuous phosphatized horizons and, based on a new age model, these are likely among some of the oldest archaeocyathan assemblages reported (Smith et al., 2016). Here, to better understand the taphonomic conditions of this exquisite preservation, we examine the sedimentology, depositional environment, and mineralogy of the strata that host these phosphatized fossiliferous horizons. Particularly, the rare preservation of phosphatized archaeocyaths allow us to examine these fossils in residue, analyze them in complementary thin sections, and, through additional mineralogical analyses, we explore the redox conditions that fostered this unusual preservation.

## 2. Geological Setting

Late Ediacaran to early Cambrian foreland basin deposits formed on the Zavkhan Terrane of southwestern Mongolia during collision of the Khantaishir-Dariv Arc and

obduction of supra-subduction zone ophiolites (Fig. 1A; Macdonald et al. 2009; Bold et al., 2013; Smith et al., ~~2015~~2016; Bold et al., 2016a, 2016b). From oldest to youngest, these strata include the Zuun-Arts, Bayangol, Salaagol, and Khairkhan formations (Fig. 1B). These foreland deposits overlie the Shuurgat Formation, which was deposited on a rifted passive margin, and record the transformation of the southwestern margin of the Zavkhan Terrane from a passive to active margin (Bold et al., 2016a, 2016b).

The Salaagol Formation is a <400 m-thick white, gray, pink, and red limestone-dominated unit that contains microbialite, ooid grainstone, archaeocyathan reefs, and minor siliciclastic beds (Voronin et al., 1982; Wood et al., 1993; Kruse et al., 1996, Smith et al., ~~2015~~2016). The thickness of the Salaagol Formation varies dramatically; in some places the formation is completely absent while in others it is composed of a ~~<~~~400 m-thick reef complex (Smith et al., ~~2015~~2016). In sections just south of Khukh-Davaa Pass (Fig. 1C), meter-scale patch reefs pinch out laterally, and locally, the Khairkhan Formation sits directly on the Bayangol Formation (Smith et al., ~~2015~~2016).

At multiple localities, the contact between the Salaagol Formation and the overlying siliciclastic-dominated Khairkhan Formation is marked by phosphatic hardgrounds that preserve archaeocyaths and SSFs. The Khairkhan Formation is composed of up to 1 km of siltstone, sandstone, and conglomerate interpreted to represent the flysch and tectonic mélange of the foreland basin (Macdonald et al., 2009; Smith et al., ~~2015~~2016). Clasts, ranging in size from pebble to boulder to km-sized and interpreted to represent olistoliths of the underlying archaeocyathan reefs, are common in this unit. Conglomerates within the Khairkhan Formation are interpreted to represent reef talus

breccia debrites, distinguishing them from conglomerate in the Bayangol Formation (Smith et al., ~~2015~~2016).

Based on species of Siberian archaeocyaths that are thought to be restricted to the Atdabanian and Botomian (Stage 2/Stage 3), ~~this unit~~the Salaagol Formation was previously assigned to this age ~~an age of Tommotian to Botomian (Fortunian to Botomian)~~ (Kruse et al., 1996); subsequent revised biostratigraphic work placed these fossils in the earliest Atdabanian (Debrenne et al. 2015; Yang et al. 2016). Recently, however, a new high-resolution carbon isotope chemostratigraphic study coupled with the complete lack of trilobite debris in the Salaagol Formation further pushes back the age of this unit to~~:~~ latest Nemakit-Daldynian and Tommotian (Fortunian/Stage 2; Smith et al., 2016~~ 2015~~). The highly $^{13}C$-enriched isotopic values documented in the lower to middle Salaagol Formation (Fig. 2A) are diagnostic of the end-Nemakit-Daldynian, and such $^{13}C$-enriched values are not found in A~~d~~tdabanian or Botomian rocks globally (Maloof et al., 2005; Smith et al., 2016). The archaeocyaths ~~in this study~~from E1221, which represent the bulk of what we studied, are from carbonates with $\delta^{13}C$ values of ~ ~~+~~-2‰, ~~just above the~~along the downturn from carbonates that record values of ~~><~~ +~~4~~7 ~~to +8~~ (Fig. 2A). The archaeocyath-bearing horizons at PARN2, however, sit in carbon isotope space that places them above those at E1221 (-2‰);~~;~~ we interpret th~~e~~is drop shown in Figure 2 from highly $^{13}C$-enriched values to $^{13}C$-depleted values~~ as~~ to approximate the Nemakit-Daldynian—Tommotian boundary (Smith et al., ~~2015~~). Because the uppermost beds of the Salaagol Formation preserve the phosphatic assemblages described herein, these fossils represent some of the earliest archaeocyaths reported, and if the chemostratigraphic age model put forth by Smith et al. (2016;

2017~~2015~~) is correct, it challenges the original biostratigraphic ranges for the Siberian archaeocyaths (e.g., Rozanov ~~v~~and Sokolov, 1980; Kirschvink and Roza~~e~~nov, 1984).

## 3. Methods

The phosphatized archaeocyaths described here were discovered while mapping new areas and measuring new sections of the Salaagol Formation. The key localities for this study are in southeast Khukh-Davaa (E1330 and PARN2) and Orolgo Gorge (E1221) (Fig. 1C, Fig. 2A). At Orolgo Gorge, the contact between the Salaagol and Khairkhan formations is covered by talus, and thus the stratigraphic context of the fossils is ~~less~~ not as precisely ~~well~~ constrained. Nonetheless, samples were collected here due to the abundance of well-preserved phosphatized fossils that were found in talus. The best-preserved and most diverse samples were collected and used in this study (E1221) (Fig. 1C). To better constrain the depositional environment of these samples, two detailed stratigraphic sections were measured and sampled that span the contact between the Salaagol and Khairkhan formations and preserve phosphatized archaeocyaths *in situ*. These sections (E1330 and PARN 2) are from two separate localities in southeast Khukh-Davaa. In both sections, carbonates were collected at high resolution throughout the entire Salaagol Formation for carbon isotope chemostratigraphy ($\delta^{13}C$) (Fig. 2A; Smith et al., ~~2015~~).

Of the samples collected at Orolgo Gorge, eight were chosen for further analysis due to their exceptional phosphatization. Portions of the samples from E1221 were dissolved in 10% buffered acetic acid and thin sectioned. The acid was changed every

other day over the course of six weeks. Residues were collected after four and six weeks. The residues were rinsed with deionized water and sieved into four fractions: >840µm, 420-840 µm, 250-420 µm, and 160-250 µm.

All residues were examined under the dissecting microscope, and fossils with different morphologies were picked. The ten best-preserved and most representative fossils from each sample were photographed under a light microscope. Fossils were sputter coated with a gold/palladium alloy and imaged at 5 kV, spot size 3 on a FEI Quanta 450 Scanning Electron Microscope (SEM). Two archaeocyath fossils showing different mineralogies were carbon coated and analyzed for Energy Dispersive Spectra (EDS) to determine composition.

Thin sections were made from each of the same eight dissolved samples, ~~in which we~~and were used to ~~observed modes of preservation~~examine~~d~~ preservation, diversity of organisms, taphonomic alteration, types of minerals, and occurrence of apatite~~phosphate~~. Samples were classified according to Dunham's classification scheme (Dunham, 1962; Embry and Klovan, 1972). ~~For the modes of preservation,~~ W~~w~~e also noted ~~whether fossils were preserved as internal molds or if they were replaced or recrystallized.~~ the distribution of apatite in the samples in thin section.

At the section E1330 in the southeast Khukh-Davaa region, 12 samples were analyzed to characterize mineralogical changes as phosphatization becomes prevalent near the Salaagol/Khairkhan contact. These samples were dissolved in a solution of 10% acetic acid buffered with 0.65 M hydrated ammonium acetate to remove some of the carbonate and concentrate the insoluble minerals. These residues were then analyzed on a Panalytical Empyrean Series 2 X-ray diffractometer operating at 40 kV and 40 mA with a

Co Kα source. Samples were mixed with acetone, and the slurries were spread onto polished 32mm Si single crystal substrates and, after air-drying, were analyzed while continuously rotated. Data were acquired from 5-85 degrees 2-theta using a step size of 0.026 degrees. Diffraction data were reduced using the HighScore Plus software suite and mineral identifications were based on correspondence to the ICDD Powder Diffraction File 4+ database. In addition, clay mineral speciation and polytype identification were performed by scanning from 69-75 degrees 2-theta using a step size of 0.026 degrees and count rates of 200 seconds per step. In this way, mineral-specific 060 reflections (i.e., glauconite, $2M_1$ illite) were quantified by peak area modeling. Using this approach, and taking advantage of the linear relationship between 060 peak area and mineral concentration, clay mineral abundances expressed as a relative fraction of the total clay content (Środoń et al., 2001).

## 4. Results

### *4.1 Stratigraphic context*

In southeast Khukh-Davaa, two sections (E1330 and PARN 2) preserve phosphatized archaeocyaths and SSFs in place (Fig. 1C, Fig. 2A, 2B). The sedimentology is very similar between the two sections, so they are plotted in a composite section in Fig. 2B. Section E1330 is about 1 km to the southeast of the second section (PARN 2). E1330 is a 16 m-thick section that contains five distinct and lenticular phosphatic horizons of archaeocyaths and SSFs ~~preserved within 10 m of bedded limestone~~ (Fig. 3A). The

phosphatic horizons are as thick as 2 cm, but pinch and swell laterally (Fig. 3B-D). At one of the phosphatic horizons, phosphatized grains and fossils fill an erosive surface (Fig. 3B). At other stratigraphic levels, phosphatic horizons splay and laterally rejoin (Fig. 3C). In strata centimeters above ~~of~~ the phosphatice hardgrounds, phosphatized fossils and grains are commonly dispersed in carbonate grainstone (Fig. 3D). The phosphatic hardgrounds and fossils are overlain by 2 m of siltstone with nodular carbonate and > 100 m of brown to black graded beds of sandstone, siltstone, and shale interpreted as turbidites of the overlying Khairkhan Formation (Smith et al., ~~2015~~).

The second detailed measured section, PARN 2, is 16 m-thick (see Fig. 2B). The bottom 10 m of the section consists of thinly bedded limestone with ~7 lenticular phosphatic horizons. All the phosphatized horizons contain a variety of fossils visible at the outcrop scale, including calcareous and phosphatized archaeocyaths and SSFs in various orientations. Similar to the strata in E1330, this interval is immediately overlain by 6 m of siltstone with nodular carbonates of the Khairkhan Formation~~. The overlying~~; the Khairkhan Formation consists of >100 m of graded beds of sandstone, siltstone, and shale with interbedded conglomerate.

Although these sections are over 1 km apart, the sedimentology of the two sections is very similar. While the number and thickness of the phosphatic horizons varies laterally, the phosphatized fossils and grains are being preserved within ~10 m of strata that record the upward progression from carbonate boundstone to graded beds of siliciclastic strata that we interpret to represent the transition from a shallow marine reef to a basinal slope environment. No phosphatized archaeocyaths were found in the Salaa Gorge section (Fig. 2A), but the Salaagol-Khairkhan contact there is similar to the

sections from southeast Khukh-Davaa. There, the Salaagol Formation grades into mixed phosphatic carbonate, which is overlain by graded beds of siliciclastic strata. Overlying this are conglomerates interpreted to represent mass-flow deposits of the Khairkhan Formation.

In Orolgo Gorge, the most distal of the sections studied (Smith et al., ~~2015~~), the phosphatized archaeocyaths were found in conglomerate above a massive microbial reef buildup, and the conglomerate is interpreted to represent a syndepositional talus slope deposit from the fore reef (Fig. 2A). ~~Some of the large talus blocks in this gorge have~~ Lenticular phosphatic lenses ~~that~~ preserve secondarily phosphatized archaeocyaths, SSFs, and grains, very similar to the sections studied in southeast Khukh-Davaa. Large clasts within the talus breccia contain archaeocyaths that are not phosphatized. We interpret these clasts as massive slump blocks (olistoliths), which fell off the flanks of the reef complexes that are preserved in more proximal sections at Salaa Gorge and southeast Khukh-Daava. ~~Overlying the covered interval with the talus blocks are large clasts, some of which contain archaeocyaths. We interpret these clasts to represent massive slump blocks and olistoliths in a talus breccia, which fell off of the flanks of massive reef complexes in the more proximal sections at Salaa Gorge and in southeast Khukh Davaa.~~

*4.2 Insoluble Residue Fossil Analysis*

Observations of the size, diversity, and abundance of skeletal material were made by examining the insoluble residues (Table 1). Although much of the residue material consists of non-biological components such as rock fragments, skeletal fragments are

present in all residues. Phosphatized archaeocyathan fragments are commonly observed in > 840 µm fraction with a minority of phosphatized chancelloriids, ~~and~~ possible hyoliths including orthothecids, and other unidentified small shelly~~id~~ fossils. SSFs are abundant in the 420-840 µm fraction. The two other size fractions did not contain much ~~articulated~~ identifiable phosphatic material, and thus were not analyzed. The vast majority of archaeocyathan fossils are preserved as phosphatic internal molds, and in some cases preserve small amounts of silica, ~~,~~ but some archaeocyathan fossils in residue are calcitic. A single green internal mold of an archaeocyath was further examined using EDS to determine elemental composition (see EDS results below).

In the internal molds, the central cavity, intersepta, ~~,~~ and pores ~~, and intersepta~~ have been filled with ~~phosphate~~ apatite (Figs. 4A—K). The intervallum, inner walls, outer walls, and septa~~e~~ ~~,~~ of archaeocyaths are rarely preserved in residues, though one fossil contained an outer wall (Fig. 4L). Some archaeocythans had a combination of phosphatized hollow spaces with a calcareous~~ified~~ outer skeleton (< 5%). The ~~majority of~~ SSFs in residue ~~are chancelloriids and hyolithids, and they~~ are preserved as internal molds ~~(Figs. 5A—D)~~ and replaced by ~~phosphate~~ apatite (Fig~~s~~. 5~~E, F~~).

*4.3 Petrographic Analysis*

Common components of all eight thin sections include micrite, skeletal fragments, peloids, intraclasts, ooids, and siliciclastic material (Table 2). Most of the matrix of the rock is micritic, and common skeletal fragments included archaeocyaths, chancelloriids, hyolith~~sids~~, ~~and~~ brachiopods, and unidentified small shelly fossils. All samples are

characterized as fossiliferous packstone. Minor siliciclastic minerals (quartz and plagioclase feldspar) are mud- to very fine-grained sand-sized, angular to subangular, and poorly sorted.

In thin section, as in residue, archaeocyathan fossils ~~are commonly both~~preserve both the calcitic exterior and phosphatic internal mold. In the examples of archaeocyaths ~~in~~filled with ~~phosphate cement~~apatite, there ~~are other grains~~is other cement, including ~~plagioclase feldspar and~~ some silica~~quartz~~, which is~~are~~ preserved inside the intervallum, central cavities, and pores of the specimens (Fig. 6A). Some ~~entirely~~ calcitic archaeocyathan skeletons without phosphatic internal molds are also present (Fig. 6B). Skeletal elements of chancelloriids and~~,~~ hyolith~~id~~s ~~and brachiopods~~ are commonly replaced by ~~phosphate~~apatite, but some calcitic examples also exist (Figs. 6C—D). ~~Phosphate~~ Apatite occurs in the internal molds, as replaced fossils, and as grains and cement (Fig. 6A, B and E). Glauconite occurs as grains (Fig. 6F), and is a common yellow-green mineral in Cambrian successions (e.g., Brasier, 1980).

*4.4 Insoluble Residue X-ray Diffractometer (XRD) Analysis and Element Dispersive Spectra (EDS)*

The mineralogical content of the insoluble residues of the twelve samples from E1330 reveal the minor minerals present during the transition from the Salaagol Formation to the Khairkhan Formation (Table 3). Quartz~~z~~, calcite and glauconite are present in all samples. In addition, clay has been identified on the basis of the position of its 060 reflection as being an Fe-rich dioctahedral variety, similar in composition to

glauconite, or Fe-rich smectites such as nontronite and saponite (Fig. 7; Moore and Reynolds, 1997). In all samples where glauconite and the Fe-rich dioctahedral clay make up 49% or more of the insoluble residue material analyzed, apatite is also present (Table 3, Fig. 8). Apatite appears in more than half of the samples, but is less abundant than glauconite and/or Fe-bearing clay.

Two fossils, one brown and one green in color, were selected under the dissecting microscope for further analysis with EDS on the SEM. The more representative brown archaeocyathan fossil had a chemical composition that included C, O, Si, P, and Ca (Fig. 9A). These elements, particularly the abundances of calcium and phosphate, are consistent with an apatite structure. The Si and O indicates some replacement by silica. The green archaeocyathan internal mold had EDS spectra that included O, Mg, Al, Si, K, Ca, and Fe (Fig. 9B). This elemental composition is consistent with glauconite.

## 5. Discussion

### *5.1 Palaeo~~E~~nvironmental Interpretations*

The Salaagol Formation is dominated by archaeocyathan reefs (Kruse et al., 1996; Smith et al., ~~2015~~), but ooid grainstone, oncolite, thrombolitic and other microbialites, and minor siliciclastic units are common throughout the formation (Fig. 2). The unit exhibits major facies changes across the Zavkhan Terrane, varying in lithology and thickness (Smith et al., ~~2015~~). In addition to sequence stratigraphy, chemostratigraphic

profiles of the Salaagol Formation in the three regions discussed in this study provide constraints on the correlations between sections (Fig. 2A; Smith et al., ~~2015~~). These data suggest that the development of the Salaagol reefs was diachronous across the basin, and that the reefs persisted for a longer period of time in Salaa Gorge and southeast Khukh Davaa than they did in Orolgo Gorge. In Salaa Gorge and southeast Khukh-Davaa, the reefs developed high relief to keep up with the transgressive systems tract, but were drowned or destroyed in deeper water sections at Orlogo Gorge by slumps coming off the flanks (Fig. 2A). These correlations imply that the horizons of phosphatized archaeocyaths from Orolgo Gorge (E1221) are slightly older than the ones from southeast Khukh-Davaa (E1330 and PARN 2). This also implies that the gradational contact between the Salaagol and Khairkhan formations is diachronous across the basin, with the phosphatic shales, silty carbonates, and reef talus of the Khairkhan Formation first appearing in the deepest water section at Orolgo Gorge.

The archaeocyaths and SSFs at the top of the formation in the southeast Khukh-Davaa (E1330 and PARN2) and Orolgo Gorge (E1221) localities, are found as disarticulated clasts in discontinuous phosphatized lenses (Fig. 3; Smith et al., ~~2015~~), suggesting transport after death. Furthermore, in hand sample, archaeocyaths and SSFs are found oriented in many different directions (Fig. 3), and in thin section, archaeocyaths are preserved with siliciclastic sediment (quartz and plagioclase feldspar) filling their cavities (Table 2; Fig. 6A). The contact between the Salaagol and Khairkhan formations is gradational with a 4 m-thick siltstone unit overlain by a 10 m-thick, thinly-bedded limestone unit with discontinuous phosphatized lenses and succeeded by an additional 2 m-thick siltstone unit with carbonate nodules (see Fig. 2). These observations, coupled

with the preservation of fossils in phosphatized transgressive lags at the base of the Khairkhan Formation, suggest that these fossils were transported from a nearby peri-reefal setting during a transgressive systems tract. This transgression is interpreted to reflect the foundering of the Salaagol reef into the axis of the foredeep basin, where deepening was accompanied by the appearance of arc-derived detritus from the orogenic wedge to the south (Smith et al., ~~2015~~).

*5.2 ~~Paleoenvironmental~~ Taphonomic Interpretations*

Previous work on the Salaagol Formation has shown that ~~Ajacicyathus archaeocyaths like~~ *Archaeolynthus, Dokidocyathus, Nochoroicyathus,* and *Rotundocyathus*, among others, were common components of archaeocyathan reefs of the Salaagol Formation (Kruse et al., 1996; Debrenne and Zhuravlev, 1996). Though most of our archaeocyathan fossils are small and incomplete, some share features with the fossils previously identified from these sections. One specimen has an outer wall preserved which is rare in our samples, and it shows simple rounded pores like those of *Archaeolynthus* (Fig. 4L), but the top of the cup is poorly preserved. Others are solitary archaeocyaths with an intervallum with straight septa, resembling those of the Nochoroicyathidae (Figs. 4D and I) (Kruse et al., 1996) (now regarded as a synonym of Ajacicyathidae, ~~*Nochoricyathidae* (Figs. 4D and I) (~~Debrenne et al., 2015~~; Kruse et al., 1996~~). The pore and septal arrangements of these phosphatized forms reveal a morphological diversity in these samples, even with incomplete specimens.

The small size and transported nature of these assemblages suggest that these archaeocyaths lived in a forereef environment. Chancelloriids and ~~hyolithids~~other benthic small shelly fossils would also have been well suited to living at the periphery of the reef, since these groups have been found in both reef and level bottom assemblages (e.g., James and Klappa, 1983; Landing, 1993; Pratt et al., 2001). The archaeocyaths and SSFs are found as broken skeletal fragments in hand sample, residue, and thin section, and the overall size of most fossil fragments is quite small, with most fossils being less than 1 cm long. Whole fossils are rare in both residue and thin section, confirming that these fossils were transported and not preserved *in situ*.

*5.3 Implications for local redox conditions*

The nature of phosphatization and associated redox conditions remain debated (e.g., Föllmi et al. 2005; Dornbos et al. 2006; Creveling et al., 2014a; 2014b). It has been suggested that ferruginous and anoxic conditions contribute to secondary apatite growth (Creveling et al., 2014a; 2014b), a condition that might have been common in Cambrian basins; however, the role of organic matter decay in providing phosphorous and controlling local redox conditions has also been proposed (e.g., Föllmi et al. 2005; Dornbos et al. 2006; März et al. 2008; Creveling et a., 2014a; 2014b). Based on the presence of phosphatic internal molds and apatite cement in the phosphatic hardgrounds described here, apatite ~~is~~ likely nucleated~~ing~~ *in situ* during transgression.

Mineralogical analyses of the insoluble residues that span the upper Salaagol Formation reveal some important patterns. Quartz is common in this analysis, which is

389 also seen in thin section as a detrital component. Calcite is also prevalent, but likely
390 reveals incomplete dissolution of the host rock. Glauconite and Fe-rich dioctahedral clay,
391 both of which are conspicuously yellow-green and easily identified in thin section, are
392 abundant in all analyzed samples, and their abundance has important implications for
393 local redox conditions. The relationship between glauconite and apatite formation is well
394 known (Odin and Létolle, 1980; Krajewski, 1984; O'Brien et al., 1990). In modern
395 environments where glauconite and apatite are forming as nodules, such as the East
396 Australian continental margin (O'Brien et al., 1990), low oxygen conditions are
397 maintained by a high organic carbon flux to the sediments. The interaction between Fe-P
398 cycling plays an important role in these settings as well, and much of these dynamics are
399 controlled by local sea level (O'Brien et al., 1990). As an analogy to Cambrian settings,
400 the part of the Salaagol where phosphatization of fossils is present co-occurs with
401 abundant glauconite. Interestingly, apatite is not abundant in all of the residues analyzed
402 from the section at E1330, which points to the patchy, lenticular nature of
403 phosphatization, something that is viewed in the field. However, glauconite and/or Fe-
404 rich dioctahedral clay are present in all analyzed samples. We suggest that these Fe-rich
405 clays, including glauconite, as well as apatite grew under low oxygen conditions, and that
406 these conditions were best maintained by a relatively high supply of organic carbon.
407 Organic carbon within the interior of the fossils likely acted as a template for apatite, and
408 in rarer instances, glauconite growth. The organic material itself may not have been a
409 sufficient source of phosphorous to account for the formation of apatite (Creveling et al.,
410 2014a), which supports the notion that these fossils were transported to an anoxic

environment where additional phosphorous was mobilized from organic rich sediments (Van Cappellean and Ingall, 1994).

We suggest that, during transgression, the archaeocyaths, which lived in oxygenated conditions, were transported to a deeper-water anoxic environment with sediment filling their cavities during transport, and then phosphate apatite grew in the pore space with other associated authigenic minerals around mineral grains (Fig. 10). In an anoxic, potentially organic-rich, deeper water setting, any remaining organic material may have thus created a site for apatite nucleation both through locally increased phosphorous availability and locally reducing conditions. Interestingly, archaeocyaths are thought to have an intervallum filled with soft-tissue (Zhuravlev, 1990; Debrenne and Zhuravlev, 1992; Wood et al., 1992), and the areas where this tissue would have decayed coincides with areas where apatitephosphate is prevalent in these archaeocyaths , both in residue and thin sections(though note the presence of apatite in the central cavity as well, in some cases). It is possible that the transgression preserved at the base of the Khairkhan Formation introduced low oxygen conditions to decaying organic matter within the transported *Ajacicyathus* archaeocyaths, creating an ideal situation for apatitephosphate to nucleate in the pore spaces. These unusual conditions represent an important early Cambrian taphonomic window and may account for the general scarcity of phosphatized archaeocyathan fossils relative to their carbonate reef-dwelling equivalents.

## 6. Conclusions

In the upper Salaagol Formation of southwestern Mongolia, archaeocyaths and SSFs were found in discontinuous phosphatized lenses. Analyses of insoluble residues and thin sections coupled with mineralogical data demonstrate that phosphatized internal molds and replaced fossils of archaeocyaths, chancelloriids, ~~and~~ hyolith~~id~~s and unidentified fossils make up the bulk of the biological components of these assemblages. The archaeocyaths and SSFs lived in a reef periphery, and were transported to a deeper marine setting during a basin-wide transgression. Sediment starvation and low oxygen conditions coupled with the decaying soft tissue in the archaeocyath's intervallum created an environment that facilitated the preservation of these fossils as phosphatic internal molds.

## LIST OF FIGURE AND TABLE CAPTIONS

**FIGURE 1**—Locality map, geological map, and generalized stratigraphy of the Zavkhan Terrane modified from Smith et al. (~~2015~~). A) Location of Zavkhan Terrane in southwestern Mongolia. B) Carbon isotope chemostratigraphic profile plotted against generalized Neoproterozoic through early Cambrian stratigraphy in the Zavkhan Terrane. The purple arrow marks where, stratigraphically, the phosphatized archaeocyath specimens were found. C) Geologic map of the Zavkhan Terrane. The purple stars mark the sample localities. (GPS Coordinates) E1330 = N 46° 58' 34.02" E 95° 34' 5.58"; E1221 = N 46° 48' 17.07" E 95° 36' 5.54"

**FIGURE 2**—Measured stratigraphic sections of the Salaagol and Khairkhan formations. A) Measured stratigraphic sections and chemostratigraphy from three of the most western localities in the Zavkhan Terrane (adapted from Smith et al., ~~2015~~). Dashed lines at the Khairkhan Formation between Orolgo and Saala gorges indicate interfingering facies B) Detailed section of composite PARN2 and E1330 stratigraphic column from southeast Khukh-Davaa showing the distribution of phosphatic lenses and phosphatized fossils at the contact between the Salaagol and Khairkhan formations.

**FIGURE 3**—Field photographs from the section near E1330 (A and B) and E1221 (C and D). A) Bedded limestone from the contact between the Salaagol and Khairkhan formations. Meter stick for scale. B) Phosphatized grains and fossils filling in a karsted cavity in the upper Salaagol Formation. C) Phosphatized lens showing both phosphatized and calcitic archaeocyaths. D) Phosphatized archaeocyaths and SSFs.

**FIGURE 4**—SEM images of phosphatized archaeocyaths. A) Branching archaeocyath. B-J) Internal molds of archaeocyaths. ~~Phosphate fills in central cavity, pores and intersepta.~~ K) Archaeocyathan pore system. L) Archaeocyath replaced by apatite. ~~Note that pores and central cavity are not filled with phosphate.~~

**FIGURE 5**—SEM images of phosphati~~c~~zed small shelly fossils. A-D) ~~Phosphatized~~ C~~c~~hancelloriid sclerites; E~~–F~~) ~~Phosphatized~~ H~~h~~yoliths; F) Possible hyolith; identification uncertain.~~ids~~.

**FIGURE 6**—Petrographic images of thin sections. All thin sections were made from the same hand samples as those used for dissolutions. A) Apatite~~Phosphate~~ filling a ~~calcified~~calcareous archaeocyath. B) ~~Calcified~~Calcareous archaeocyath (left) and ~~calcified~~calcareous archaeocyath filled with apatite~~phosphate~~ (right). C) Phosphatized hyolithid (black arrow). D) ~~Calcified~~Calcareous ~~chancelloriid~~small shelly fossil. E) Possible phosphatic brachiopod shell in the center of the picture, and p~~P~~hosphatic cement (white arrow). F) Glauconitic cement (black arrow).

**FIGURE 7**—X-ray diffraction profile for a glauconitic sample, E1330-1. The high angle portion of the profile (top; between 70-74 degrees) reveals the presence of an iron-rich dioct~~a~~ehedral clay, which is also abundant in these residues and contains slightly more iron than glauconite. The bottom panel shows the parent profile.

**FIGURE 8~~7~~**—X-ray diffraction profile from two samples showing high and low abundances of apatite at the top and bottom, respectively (E1330-12.5 and E1330-2). All dashed lines correspond to apatite peaks. Quartz and calcite peaks are also indicated.

~~**FIGURE 8**—X-ray diffraction profile for a glauconitic sample, E1330-1. The high angle portion of the profile (top; between 70-74 degrees) reveals the presence of an iron-rich~~

~~dioctehedral clay, which is also abundant in these residues and contains slightly more iron than glauconite.~~

**FIGURE 9**—Modes of preservation of archaeocyaths. A) Brown, phosphatized archaeocyath 3A2.20.11 under the light microscope. This specimen is similar to many of the other fossils in residue. The EDS spectra of C, O, Si, P and Ca is consistent with the fossil being composed of apatite and silica. B) Green, glauconitized archaeocyath 5A2.20.3 under the light microscope. The EDS spectra of C, O, Mg, Al, Si, K, Ca, and Fe is consistent with glauconite.

**FIGURE 10**—Schematic model for the phosphatization process of archaeocyaths A) *In situ* archaeocyath. B) Archaeocyath transported from forereef environment to a deeper marine setting. C) Anoxic conditions and soft tissue decay create a nucleation site for apatite to grow. Phosphatic internal mold forms.

**TABLE 1**—Qualitative Residue Descriptions of >840µm and 420 µm to 840 µm. In >840µm sieve sizes, phosphatized archaeocyaths are found in all residue samples except for E1221.6A1.20, which did not yield any fossils. In all >840µm residue samples, apatite~~phosphate~~ and calcite are observed. Residue sample E1221.5A2.20 has a single glauconitic archaeocyath. In the smaller sieve sizes of 420 µm to 840 µm, phosphatized and calcitic archaeocyaths are observed in all 16 residues. Three residues, E1221.4A2.40, E1221.6A2.40, and E1221.8A2.40 have a majority of phosphatized chancelloriids and phosphatized archaeocyaths. Phosphatized hyolithids, phosphatized chancelloriids, and phosphatized archaeocyaths yield the majority of fossils in residue sample E1221.6A2.40.

**TABLE 2**— Qualitative Petrographic Descriptions. All 8 thin sections are observed under the petrographic microscope, and all rock samples are classified as fossiliferous packstone.

**TABLE 3—**Mineralogical compositions of the insoluble residues from x-ray diffraction analysis of twelve samples from section E1330 in the southeast Khukh-Davaa area ~~from x-ray diffraction analysis~~.

## ACKNOWLEDGMENTS

We thank the Smith College Praxis Summer Internship, the Smith College Tomlinson Fund, NASA MIT Astrobiology node, NASA Geobiology grant NNH10ZDA001N-EXO, and NSF GRF to E. Smith for financial support. We thank U. Bold, M. Delger, M. Jugder, A. Dorj, O. Dandar, U. Khuchitbaatar, T. Petach, and E. Smith for field assistance. We thank M. Vollinger, E. Hall, S. Westacott, W. Feng, and E. Perlmutter for lab support, and J. Wopereis and J. Brady for SEM and EDS training. C. Dwyer also acknowledges the Pruss lab members for encouragement.

## REFERENCES


~~Alexander, E.M., and Gravestock, D.I., 1990, Sedimentary facies in the Sellick Hill Formation, Fleurieu Peninsula, South Australia, *in* Jago, J.B., and Moore, P.S., eds., The Evolution of a Late Precambrian- Early Palaeozoic Rift Complex: The Adelaide Geosyncline: Australia, Special Publication Geological Society, p. 269-289.~~

Bengtson, S., and Yue, Z., 1997. Fossilized metazoan embryos from the Earliest Cambrian: Science. 277, 1645-1648. doi: 10.1126/science.277.5332.1645.

Bold, U., Macdonald, F.A., Smith, E.F., Crowley, J.L., and Minjin, C., 2013. Elevating the Neoproterozoic Tsagaan-Olom Formation to a Group. Mongolian Geoscientist. 39, 1-6.

Bold, U., Crowley, J.L., Smith, E.F., Sambuu, O., and Macdonald, F.A., 2016b. Neoproterozoic to early Paleozoic tectonic evolution of the Zavkhan terrane of Mongolia: Implications for continental growth in the Central Asian orogenic belt. Lithosphere. 8, 729-750. doi:10.1130/L549.1.

Bold, U., Smith, E.F., Rooney, A.D., Bowring, S.A., Buchwaldt, R., Dudás, F.Ö., Ramezani, J., Crowley, J.L., Schrag, D.P., and Macdonald, F.A., 2016a. Neoproterozoic stratigraphy of the Zavkhan terrane of Mongolia: The backbone for Cryogenian and early Ediacaran chemostratigraphic records. American Journal of Science. 316, 1-63. doi: 10.2475/01.2016.01.

Brasier, M.D., Shields, G., Kuleshov, V.N., and Zhegallo, E.A., 1996. Integrated chemo- and biostratigraphic calibration of early animal evolution: Neoproterozoic–early Cambrian of southwest Mongolia. Geological Magazine. 133, 445–485. https://doi.org/10.1017/S0016756800007603.

Brasier, M.D., 1980. The Lower Cambrian transgression and glauconite-phosphate facies in western Europe. Journal of the Geological Society of London. 137, 695-703. doi: 10.1144/gsjgs.137.6.0695.

Butterfield, N. J., 2003. Exceptional fossil preservation and the Cambrian explosion. Integrative and Comparative Biology. 43, 166–177. doi: 10.1093/icb/43.1.166.

Cook, P. J., 1992. Phosphogenesis around the Proterozoic-Phanerozoic transition. Journal of the Geological Society. 149, 615–620. doi: 10.1144/gsjgs.149.4.0615.

Creveling, J. R., Johnston, D. T., Poulton, S. W., Kotrc, B., März, C., Schrag, D. P., and Knoll, A. H., 2014a. Phosphorus sources for phosphatic Cambrian carbonates. Geological Soceity of America Bulletin. 126, 145–163. doi: 10.1130/B30819.1.


Commented [Office1]: Be consistent with doi: XXX

Creveling, J. R., Knoll, A. H., and Johnston, D. T., 2014b. Taphonomy of Cambrian phosphatic small shelly fossils. Palaios. 29, 295-308. http://dx.doi.org/10.2110/palo.2014.002.

~~Debrenne, F., 2007, Lower Cambrian archaeocyathan bioconstructions: C.R. Palevol, v. 6, p. 5-19.~~

Debrenne, F., and Vacelet, J., 1984. Archaeocyatha: Is the sponge model consistent with their structural organisation?. Palaeonto-graphica Americana. 54, 358–369.

Debrenne, F., and Zhuravlev, A.Yu., 1992. Irregular Archaeocyaths. Cahiers de Paléontologie Éditions du Centre National de la Recherche Scientifique, Paris, pp. 218.

Debrenne, F. and Zhuravlev, A. Yu., 1996. Archaeocyatha, palaeoecology: a Cambrian sessile fauna,. i~~I~~n ~~A.~~ Cherchi, A. (E~~e~~d.), Autecology of Selected Fossil Organisms: Achievements and Problems. Bollettino della Societa Paleontologica Italiana, Modena, pp. 77-85. ~~Bollettino della Societa Paleontologica Italiana, Modena.~~

~~Debrenne, F., and Zhuravlev, A.Y., 1996, Archaeocyatha, Cambrian sessile fauna: Bolletino Societa Paleontologoica Italiana, v. 3, p. 1-7.~~

Debrenne, F., Hartman, W. D., Kershaw, S., Kruse, P. D., Nestor, H. Rigby Sr., J. K., Senowbari-Daryan, B., Stearn, C. W., Stock, C. W., Vacelet, J., Webby, B. D., West, R. R., Willenz, P., Wood, R. A., Zhuravlev, A. Yu., ~~DeBrenne et al.,~~ 2015. Part E Porifera, Revised, Hypercalcified porifera, Volumes 4 and 5, ~~Hypercalcified Porifera,~~ in Moore, R. C. (Eds.), Treatise on Iinvertebrate Ppaleontology, Volume 4, ~~Boulder, Colorado,~~ Geological Society of America (and University of Kansas Press), Boulder, Colorado, pp. 1223.

Dornbos, S. Q., Bottjer, D. J., Chen, J., Gao, F., Oliveri, P., and Li, C., 2006. Environmental controls on the taphonomy of phosphatized animals and animal embryos from the Neoproterozoic Doushantuo Formation, southwest China. Palaios. 21, 3–14. doi: 10.2110/palo.2004.p04-37.

Dunham, R.J., 1962. Classification of Carbonate Rocks According to Depositional Texture, in: Ham, W.E. (Eds.), Classification of Carbonate Rocks- A Symposium. American Association of Petroleum Geologists, Norman, pp. 108-121.

Dzik, J., 1994. Evolution of 'small shelly fossils' assemblages of the early Paleozoic. Acta Palaeontologica Polonica. 39, 247–313.

Embry, A.F., and Klovan, J.E., 1972. Absolute water depth limits of Late Devonian paleoecological zones. Geologische Rundschau. 61, 672-686.

Esakova, N.V.-, and Zhegallo, E.A., 1996. Biostratigraphy and fauna of the Lower Cambrian of Mongolia. Trudy, Sovmestnaya Rossiysko-Mongol'skaya Paleontologicheskaya Ekspeditsiya. 46, 1–214.

Föllmi, K. B., Badertscher, C. De Kaenel, E., Stille, P., John, C. M., Adatte, T., and Steinmann, P. 2005. Phosphogenesis and organic-carbon preservation in the Miocene Monterey Formation at Naples Beach, California– The Monterey hypothesis revisited. Geological Society of America Bulletin. 117, 589–619. doi: 10.1130/B25524.1.

Grotzinger, J.P., and James, N.P., 2000. Precambrian carbonates: evolution of understanding, in Grotzinger, J.P., and James, N.P. (Eds.), Carbonate Sedimentation and Diagenesis in the Evolving Precambrian World. Society of Sedimentary Geology (SEPM), Tulsa, Special Publication 67, pp. 3–20. doi: 10.2110/pec.00.67.0003.

James, N.P., and Klappa, C.F., 1983. Petrogenesis of Early Cambrian reef limestones, Labrador, Canada. Journal of Sedimentary Petrology. 53, 1051-1096. doi: 10.1306/212F831E-2B24-11D7-8648000102C1865D.

Kirschvink, J. L., and Rozanov, A. Yu., 1984. Magnetostratigraphy of lower Cambrian strata from the Siberian Platform: a palaeomagnetic pole and a preliminary polarity time-scale. Geological Magazine. 121, 189-203.

Krajewski, K. P. 1984. Early diagenetic phosphate cements in the Albian condensed glauconitic limestone of the Tatra Mountains, Western Carpathians. Sedimentology. 31, 443-470. doi: 10.1111/j.1365-3091.1984.tb01812.x

Kruse, P. D., 1990. Are archaeocyaths sponges, or are sponges archaeocyaths?. Special Publication–Geological Society of Australia. 16, 310–323.

~~Kruse, P. D, Zhuravlev, A. Y., James, N. P. 1995, Primordial metazoan-calcimicrobial reefs: Tommotian (Early Cambrian) of the Siberian Platform, PALAIOS, v. 10, p. 291-321.~~

Kruse, P. D., Gandin, A., Debrenne, F., and Wood, R., 1996. Early Cambrian bioconstructions in the Zavkhan Basin of western Mongolia. Geological Magazine. 133, 429–444. https://doi.org/10.1017/S0016756800007597.

Landing, E., 1993. *In situ* earliest Cambrian tube worms and the oldest metazoan-constructed biostrome (Placentian Series, southeastern Newfoundland). Journal of Paleontology. 67, 333-342.

637 Macdonald, F.A., Jones, D.S., and Schrag, D.P., 2009. Stratigraphic and tectonic
638 implications of a newly discovered glacial diamictite–cap carbonate couplet in
639 southwestern Mongolia. Geology. 37, 123–126. doi:10.1130/G24797A.1; 3.

640 Maloof, A. C., Schrag, D. P., Crowley, J. L., and Bowring, S. A., 2005. An expanded
641 record of Early Cambrian carbon cycling from the Anti-Atlas Margin, Morocco,
642 Candian Journal of Earth Sciences. 42, 2195-2216. doi: 10.1139/E05-062.

643 März, C., Poutlon, S. W., Beckmann, B., Küster, K., Wagner, W., and Kasten, S., 2008.
644 Redox sensitivity of P cycling during marine black shale formation: Dynamics of
645 sulfidic and anoxic, non-sulfidic bottom waters. Geochimica and Cosmochimica
646 Acta. 72, p. 3703-3717. https://doi.org/10.1016/j.gca.2008.04.025.

647 Moore, D. M., and Reynolds Jr., R. C., 1997. X-Ray diffraction and the indetification and
648 analysis of clay minerals, second ed. Oxford University Press, New York, pp.
649 378.

650 Myrow, P. M., Pope, M. C., Goodge, J. W., Fischer, W., and Palmer, A. R., 2002.
651 _____Depositional history of pre-Devonian strata and timing of Ross orogenic
652 _____tectonism in the central Transantarctic Mountains, Antarctica. Geological Society
653 _____of American Bulletin. 114, 1070–1088. doi:10.1130/0016-
654 _____7606(2002)114<1070:DHOPDS>2.0.CO;2.
655

656 O'Brien, G. W., Milnes, A. R., Veeh, H. H., Heggie, D. T., Riggs, S. R., Cullen, D. J.,
657 Marshall, J. F., and Cook, P. J., 1990. Sedimentation dynamics and redox iron-
658 cycling: Controlling factors for the apatite—glauconite association on the east
659 Australian continental margin. Geological Society, London, Special Publications.
660 52, 61-86.

661 Odin, G. S., and Létolle, R., 1980. Glauconization and phosphatization environments: a
662 tentative comparison, in Bentor, Y.K (Ed), SEPM Special Publication 29. Society
663 of Economic Paleontologists and Mineralogists, Tulsa, pp. 227-237.
664
665 Porter, S. M., 2004. Halkieriids in Middle Cambrian phosphatic limestones from
666 _____Australia. Journal of Paleontology. 78, 574–590. doi: 0022-3360/04/0078-574.
667

668 Pratt, B.R., Spincer, B.R., Wood, R., and Zhuravlev, A.Yu., 2001. Ecology and evolution
669 of Cambrian reefs, in: Zhuravlev, A.Yu., and Riding, R., (Eds.), The Ecology of
670 the Cambrian Radiation. Columbia University Press, New York, pp. 254-274.

671 Rigby, J.K., and Gangloff, R.A., 1987. Phylum Archaeocyatha, in: Boardman, R.S.,
672 Cheetham, A.H., and Rowell, A.J., (Eds.), Fossil Invertebrates. Blackwell, Palo
673 Alto, pp. 107-115.

674 Rowland, S. M., and Gangloff, R. A., 1988. Structure and paleoecology of Lower
675 _____Cambrian reefs. Palaios. 3, 111–135. http://dx.doi.org/10.2307/3514525.

~~Rowland, S.M., 2001, Archaeocyaths: A History of Phylogenetic Interpretation: Journal of Paleontology, v. 75, p. 1065-1078.~~

Rozanov, A. Yu., and Sokolov, B.S., 1980. The p~~P~~roblem of the Precambrian-Cambrian boundary. Geological Magazine. 117, 23-27.

Skovsted, C. B., 2006., Small shelly fauna from the Upper Lower Cambrian Bastion and Ella Island formations, North-East Greenland.: Journal of Paleontology., 80,1087–1112.

Smith, E.F., Macdonald, F.A., Petach, T.A., Bold, U., and Schrag, D.P., 2016 ~~2015~~., Integrated ___stratigraphic, geochemical, and paleontological late Ediacaran to early Cambrian ___records from southwestern Mongolia.: Geological Society of America Bulletin., ~~v.~~ 128, ~~p.~~ 442-468. doi: 10.1130/B31248.1.

Smith, E. F., Macdonald, F. A., Petach, T. A., and Bold, U., 2017. Integrated stratigraphic, geochemical, and paleontological late Ediacaran to early Cambrian records from southwestern Mongolia: Reply. Geological Society of America Bulletin. 129, doi: 10.1130/B31763.1

~~doi: 10.1130/B31248.1.~~

Środoń J., Drits V.A., McCarty D.K., Hsieh J.C., Eberl D.D., ~~(~~2001.~~)~~ Quantitative x-ray diffraction analysis of clay-bearing rocks from random preparations. Clays and Clay Minerals. 49, 514-528.

Van Capellen, P., and Ingall, E. D., 1994. Benthic phosphorus regeneration, net primary production, and ocean anoxia: A model of the coupled marine biogeochemical cycles of carbon and phosphorus. Paleoceanography. 9, 677-692.

Voronin, Yu.I., Voronova, L.G., Grigor'eva, N.V., Drozdova, N.A., Zhegallo, E.A., Zhuravlev, A.Yu., Ragozina, A.L., Rozanov, A.Yu., Sayutina, T.A., Sysoev, V.A., Fonin, V.D., 1982. The Precambrian/Cambrian boundary in the geosynclinal areas (Salaany-Gol reference section, MPR). Sovmestnaya Sovetsko-Mongol'skaya Paleontologicheskaya Ekspeditsiya, Trudy. 18, 1-150.

~~: Moscow, Akademia Nauk SSSR,Trudy Sovmestnoy Sovetsoko-Mongol'skoy Paleontologicheskoy Ekspeditsii, 150 p.~~

Wang, X., Zhang, Z., and Han, J., 2012. Cyanobacteria fossils and the microborings on the archaeocyathids from the Shuijingtuo Formation of the Cambrian (Series 2), Yichang, Hubei Province. Acta Micropalaeontologica Sinica. 29, 170-178.

Wang, Y., Li, Y., and Zhang, Z., 2010., Note on small skeletal fossils from the uppermost Shuijingtuo formation (Early Cambrian) in the Yangtze Gorge area.: Acta Palaeontologica Sinica., ~~v.~~ 49, ~~p.~~ 511–523.

**Commented [SP2]:** I see a Rozanov and Sokolov 1980 but not a Rozanov 1980. Please fill in this reference.

Wood, R., 1990., Reef-building sponges.: American Scientist. 7, v. 78, p. 224–235.

Wood, R., Zhuravlev, A. Yu., and Anaaz, C.T., Tseren, CAnaaz, C.T., 1993., The ecology of Lower Cambrian buildups from Zuune Arts, Mongolia: implications for early metazoan reef evolution.: Sedimentology., v. 40, p. 829–858. doi:10.1111/j.1365-3091.1993.tb01364.x.

Wood, R., Zhuravlev, A. Yu., and Debrenne, F., 1992. Functional biology and ecology of archaeocyatha. Palaios. 7, 131–156. doi: 10.2307/3514925.

Wrona, R., 2004., Cambrian microfossils from glacial erratics of King George Island, Antarctica.: Acta Palaeontologica Polonica., v. 49, p. 13–56.

Xiao, S. H., and Knoll, A. H., 2000. Phosphatized animal embryos from the Neoproterozoic Doushantuo formation at Weng'an, Guizhou, South China. Journal of Paleontology. 74, 767–788.

Yang, A., Zhu, M., Zhuravlev, A. Yu., Yuan, K., Zhang, J., Chen, Y., 2016. Archaeocyathan zonation of the Yangtze Platform: Implications for regional and global correlation of lower Cambrian stages. Geological Magazine. 153, 388-409. https://doi.org/10.1017/S0016756815000333

Zhang, Z.-F., Zhang, Z.-L., Li, G.-X., and Holmer, L. E., 2016. The Cambrian brachiopod fauna from the first-trilobite age Shuijingtuo Formation in the Three Gorges area of China. Paleoworld. 25, 333-355. https://doi.org/10.1016/j.palwor.2015.10.001.

Zhuravlev, A. Yu., 1989., Poriferan aspects of archaeocyathan skeletal function. : proceedings of the sixth conference on fossil Cnidaria: Memoir Association of Australasianian Paleontologists., v. 8, p. 387–399.

Zhuravlev, A. Yu., 1990., Sistema arkheotsiat [Systematics of archaeocyaths], in: Menner, V.V. (, Eed.), Sistematika i filogeniya bespozvonochnykh: Kriterii vydeleniya vysshikh taksonov [Systematics and phylogeny of invertebrates: Criteria of high taxa establishing]. Nauka, Moscow, pp. 28-54.

Highlights

Archaeocyaths from the lower Cambrian of southwestern Mongolia were investigated.

Archaeocyaths and associated small shelly fossils (SSFs) are phosphatized.

The minerals in the assemblages suggest transportation to a low oxygen setting.

Analysis of these fossils links taphonomy to paleoenvironment of preservation.

## LIST OF FIGURE AND TABLE CAPTIONS

**FIGURE 1**—Locality map, geological map, and generalized stratigraphy of the Zavkhan Terrane modified from Smith et al. (2016). A) Location of Zavkhan Terrane in southwestern Mongolia. B) Carbon isotope chemostratigraphic profile plotted against generalized Neoproterozoic through early Cambrian stratigraphy in the Zavkhan Terrane. The purple arrow marks where, stratigraphically, the phosphatized archaeocyath specimens were found. C) Geologic map of the Zavkhan Terrane. The purple stars mark the sample localities. (GPS Coordinates) E1330 = 46° 58’ 34.02” N 95° 34’ 5.58” E; E1221 = 46° 48’ 17.07” N 95° 36’ 5.54” E

**FIGURE 2**—Measured stratigraphic sections of the Salaagol and Khairkhan formations. A) Measured stratigraphic sections and chemostratigraphy from three of the most western localities in the Zavkhan Terrane (adapted from Smith et al., 2016). Dashed lines at the Khairkhan Formation between Orolgo and Saala gorges indicate interfingering facies B) Detailed section of composite PARN2 and E1330 stratigraphic column from southeast Khukh-Davaa showing the distribution of phosphatic lenses and phosphatized fossils at the contact between the Salaagol and Khairkhan formations.

**FIGURE 3**—Field photographs from the section near E1330 (A and B) and E1221 (C and D). A) Bedded limestone from the contact between the Salaagol and Khairkhan formations. Meter stick for scale. B) Phosphatized grains and fossils filling in a karsted cavity in the upper Salaagol Formation. C) Phosphatized lens showing both phosphatized and calcitic archaeocyaths. D) Phosphatized archaeocyaths and SSFs.

**FIGURE 4**—SEM images of phosphatized archaeocyaths. A) Branching archaeocyath. B-J) Internal molds of archaeocyaths. K) Archaeocyathan pore system. L) Archaeocyath replaced by apatite.

**FIGURE 5**—SEM images of phosphatic small shelly fossils. A-D) Chancelloriid sclerites; E) Hyoliths; F) Possible hyolith; identification uncertain..

**FIGURE 6**—Petrographic images of thin sections. All thin sections were made from the same hand samples as those used for dissolutions. A) Apatite filling a calcareous archaeocyath. B) Calcareous archaeocyath (left) and calcareous archaeocyath filled with apatite (right). C) Phosphatized hyolithid (black arrow). D) Calcareous small shelly fossil. E) Possible phosphatic brachiopod shell in the center of the picture, and phosphatic cement (white arrow). F) Glauconitic cement (black arrow).

**FIGURE 7**—X-ray diffraction profile for a glauconitic sample, E1330-1. The high angle portion of the profile (top; between 70-74 degrees) reveals the presence of an iron-rich dioctahedral clay, which is also abundant in these residues and contains slightly more iron than glauconite. The bottom panel shows the parent profile.

**FIGURE 8**—X-ray diffraction profile from two samples showing high and low abundances of apatite at the top and bottom, respectively (E1330-12.5 and E1330-2). All dashed lines correspond to apatite peaks. Quartz and calcite peaks are also indicated.

**FIGURE 9**—Modes of preservation of archaeocyaths. A) Brown, phosphatized archaeocyath 3A2.20.11 under the light microscope. This specimen is similar to many of the other fossils in residue. The EDS spectra of C, O, Si, P and Ca is consistent with the fossil being composed of apatite and silica. B) Green, glauconitized archaeocyath

5A2.20.3 under the light microscope. The EDS spectra of C, O, Mg, Al, Si, K, Ca, and Fe is consistent with glauconite.

**FIGURE 10**—Schematic model for the phosphatization process of archaeocyaths A) *In situ* archaeocyath. B) Archaeocyath transported from forereef environment to a deeper marine setting. C) Anoxic conditions and soft tissue decay create a nucleation site for apatite to grow. Phosphatic internal mold forms.

**TABLE 1**—Qualitative residue descriptions of >840 μm and 420 μm to 840 μm.

**TABLE 2**— Qualitative petrographic descriptions from thin sections.

**TABLE 3—**Mineralogical compositions of the insoluble residues from x-ray diffraction

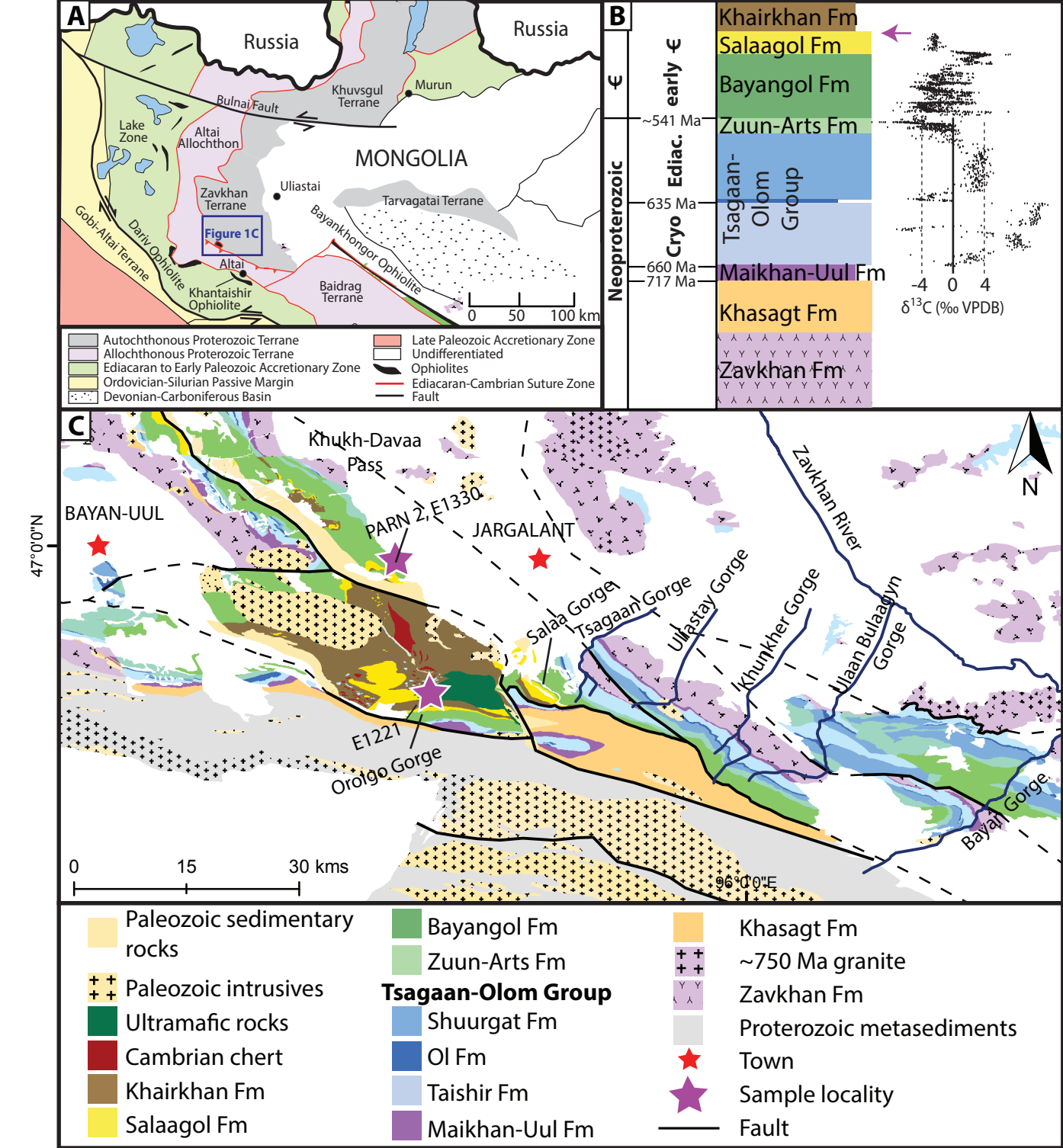
A
Russia
Russia
Khuvsgul Terrane
Murun
Bulnai Fault
Lake Zone
Altai Allochthon
MONGOLIA
Zavkhan Terrane
Uliastai
Tarvagatai Terrane
Figure 1C
Bayankhongor Ophiolite
Gobi-Altai Terrane
Darlv Ophiolite
Altai
Khantaishir Ophiolite
Baidrag Terrane
0 50 100 km
Autochthonous Proterozoic Terrane
Allochthonous Proterozoic Terrane
Ediacaran to Early Paleozoic Accretionary Zone
Ordovician-Silurian Passive Margin
Devonian-Carboniferous Basin
Late Paleozoic Accretionary Zone
Undifferentiated
Ophiolites
Ediacaran-Cambrian Suture Zone
Fault
B
Neoproterozoic
Cryo
Ediac.
Є
early Є
~541 Ma
635 Ma
660 Ma
717 Ma
Khairkhan Fm
Salaagol Fm
Bayangol Fm
Zuun-Arts Fm
Tsagaan-Olom Group
Maikhan-Uul Fm
Khasagt Fm
Zavkhan Fm
-4 0 4
δ13C (‰ VPDB)
C
47°0'0"N
Khukh-Davaa Pass
BAYAN-UUL
PARN 2, E1330
JARGALANT
Salaa Gorge
Tsagaan Gorge
Ulastay Gorge
Khunkher Gorge
Ulaan Bulaagyn Gorge
Zavkhan River
N
E1221
Orolgo Gorge
Bayan Gorge
0 15 30 kms
96°0'0"E
Paleozoic sedimentary rocks
Paleozoic intrusives
Ultramafic rocks
Cambrian chert
Khairkhan Fm
Salaagol Fm
Bayangol Fm
Zuun-Arts Fm
Tsagaan-Olom Group
Shuurgat Fm
Ol Fm
Taishir Fm
Maikhan-Uul Fm
Khasagt Fm
~750 Ma granite
Zavkhan Fm
Proterozoic metasediments
Town
Sample locality
Fault

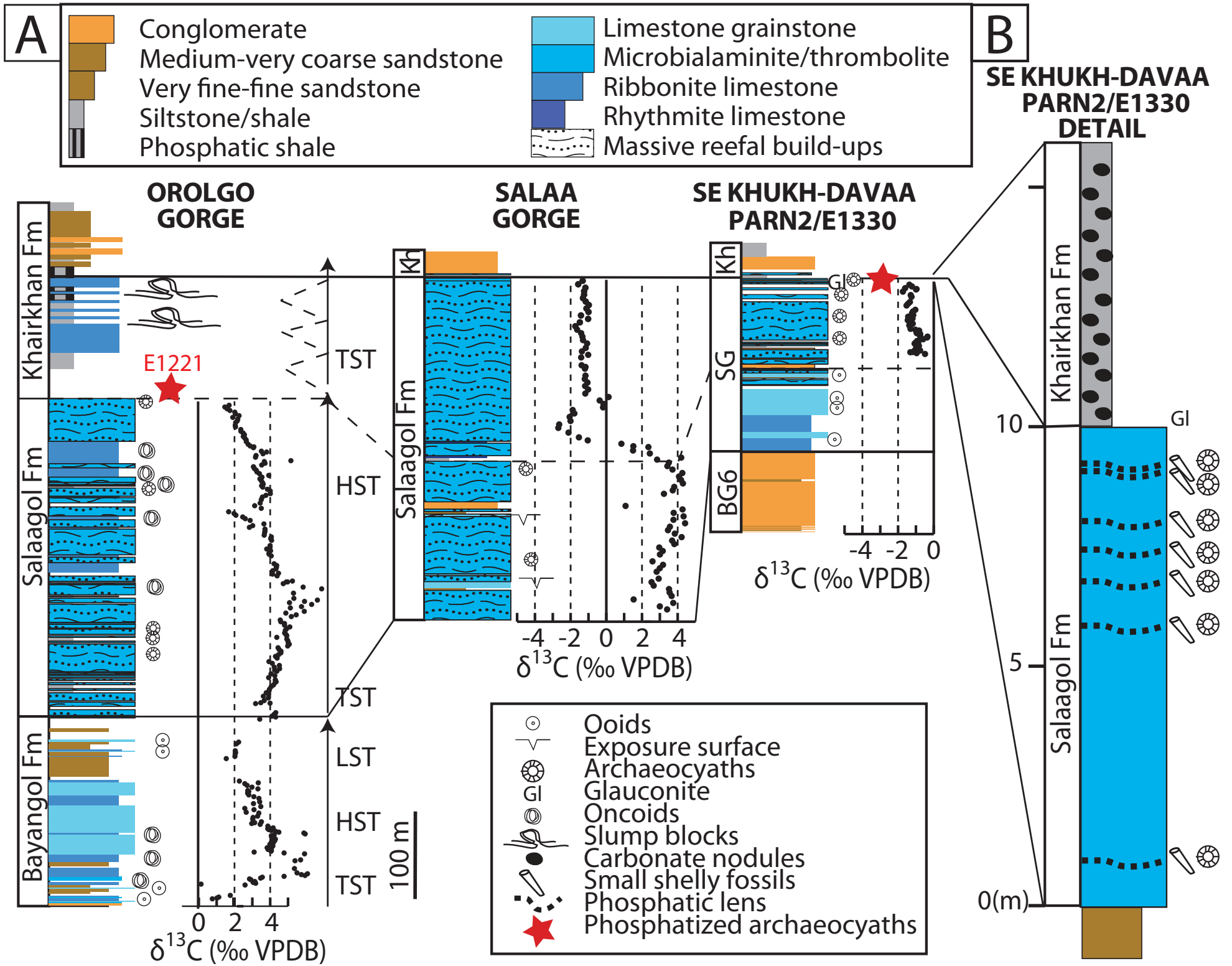
A
Conglomerate
Medium-very coarse sandstone
Very fine-fine sandstone
Siltstone/shale
Phosphatic shale
Limestone grainstone
Microbialaminite/thrombolite
Ribbonite limestone
Rhythmite limestone
Massive reefal build-ups
B
SE KHUKH-DAVAA
PARN2/E1330
DETAIL
OROLGO
GORGE
SALAA
GORGE
SE KHUKH-DAVAA
PARN2/E1330
Khairkhan Fm
Salaagol Fm
Bayangol Fm
E1221
TST
HST
TST
LST
HST
TST
100 m
Kh
SG
BG6
Gl
0 2 4
δ13C (‰ VPDB)
-4 -2 0 2 4
δ13C (‰ VPDB)
-4 -2 0
δ13C (‰ VPDB)
10
5
0(m)
Ooids
Exposure surface
Archaeocyaths
Glauconite
Oncoids
Slump blocks
Carbonate nodules
Small shelly fossils
Phosphatic lens
Phosphatized archaeocyaths

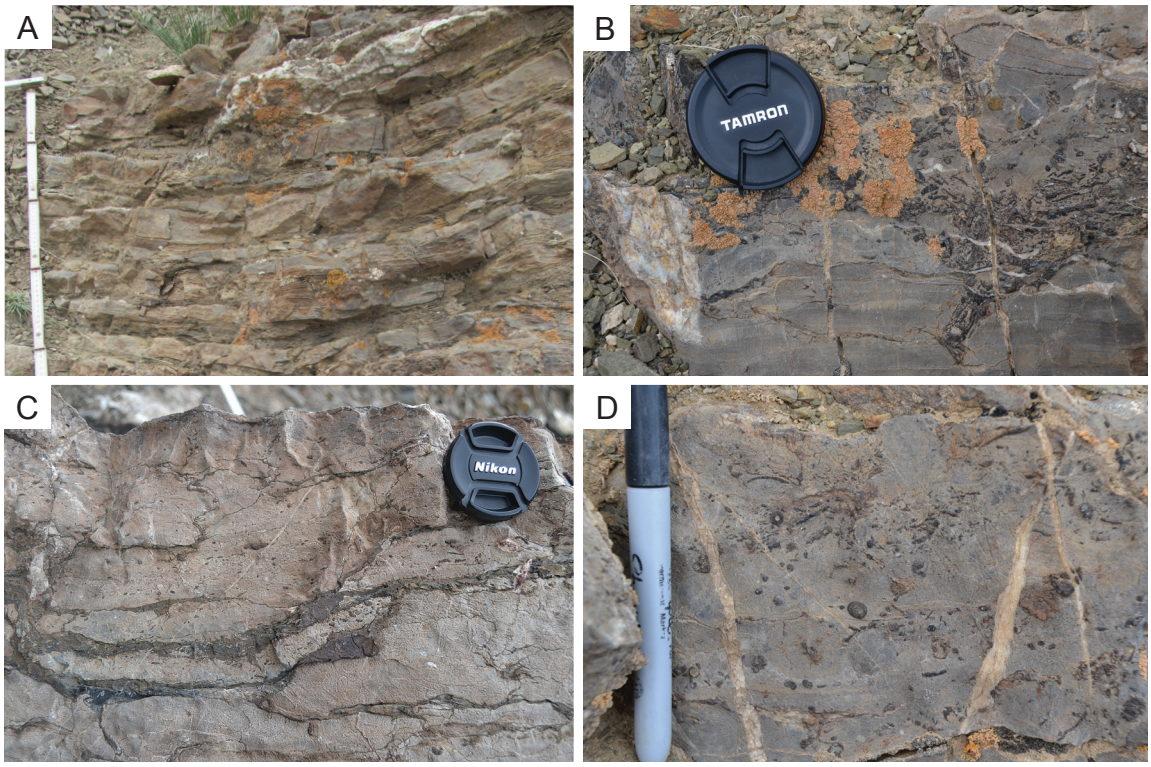
A
B
TAMRON
C
Nikon
D

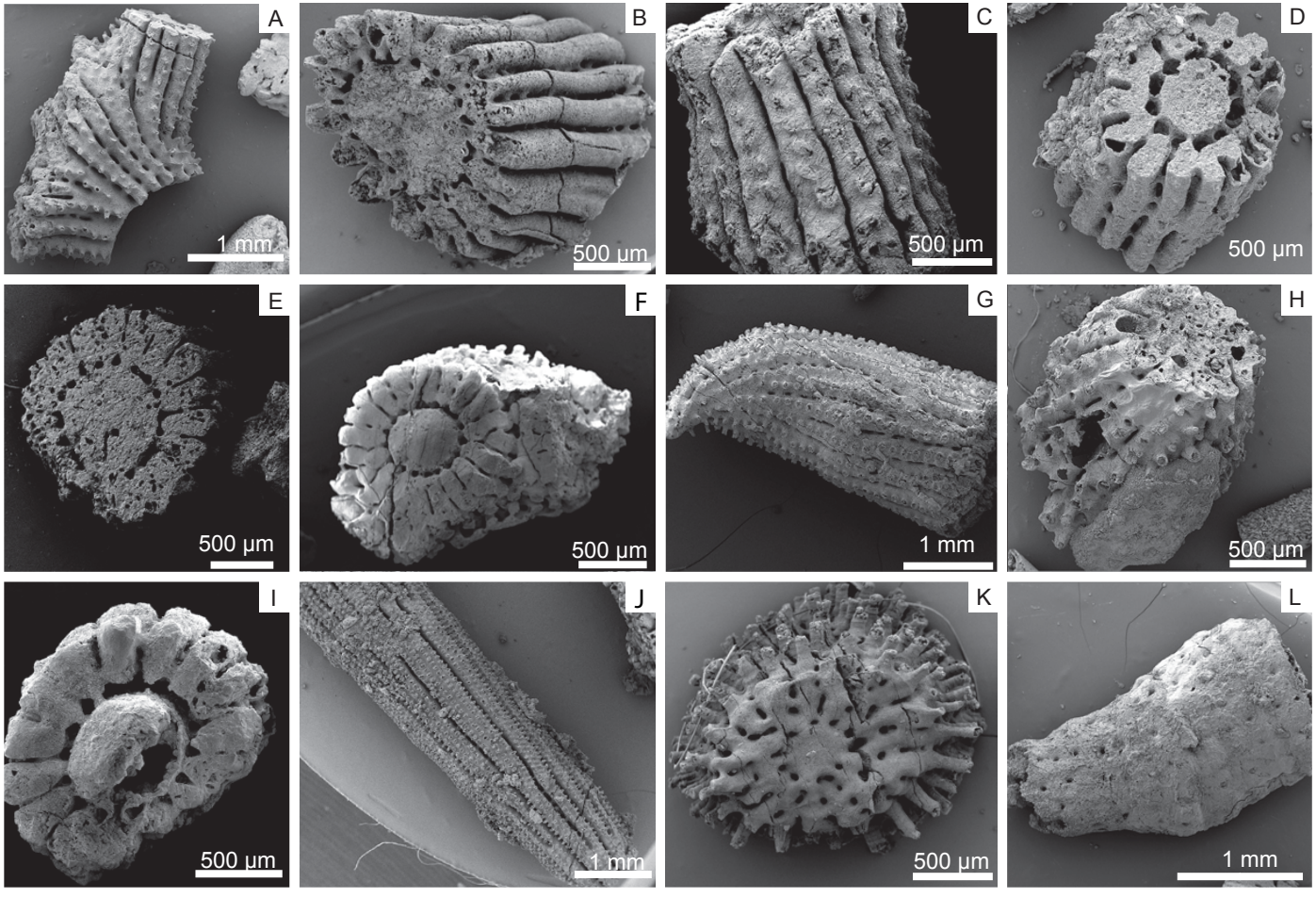
A
1 mm
B
500 µm
C
500 µm
D
500 µm
E
500 µm
F
500 µm
G
1 mm
H
500 µm
I
500 µm
J
1 mm
K
500 µm
L
1 mm

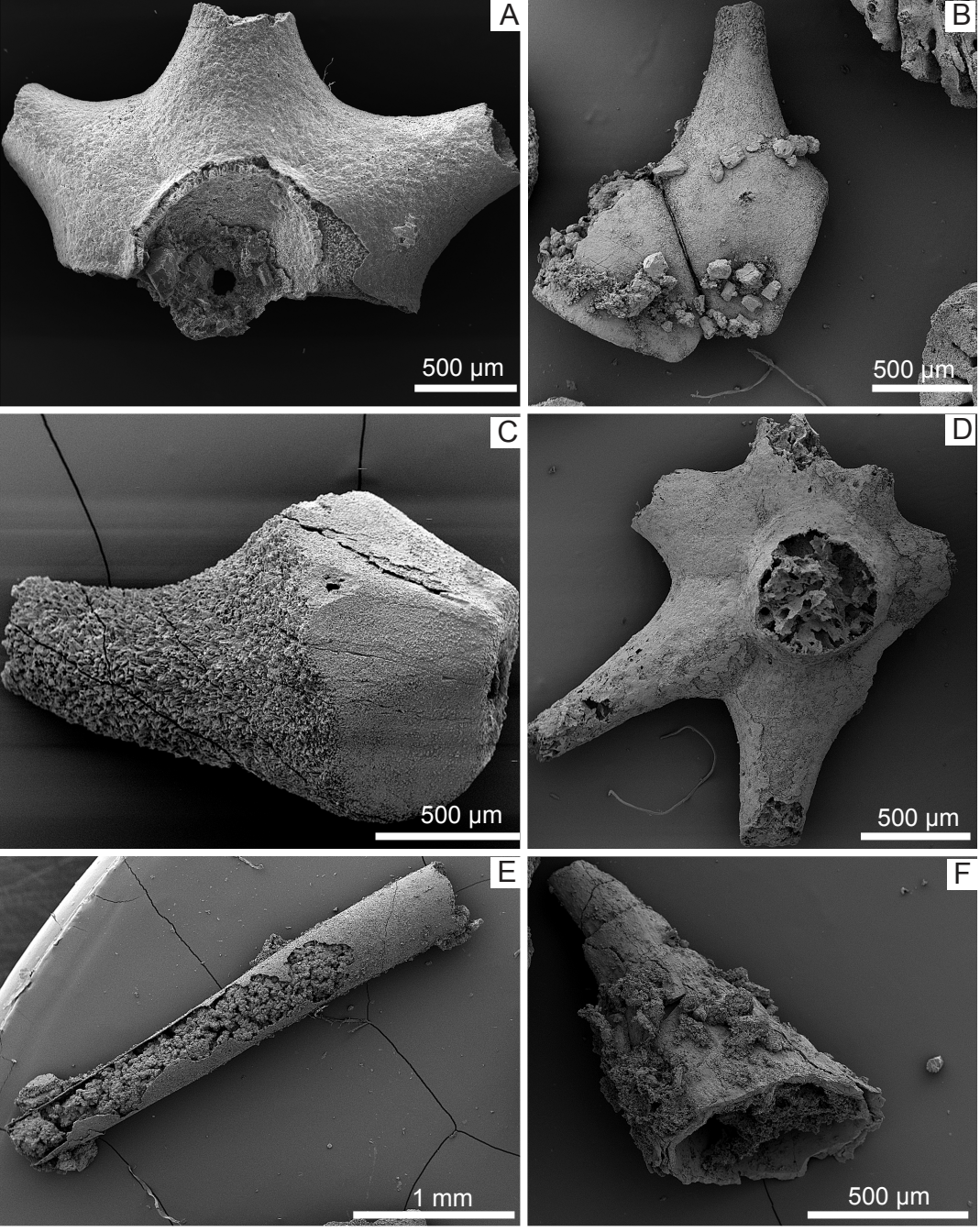
A
500 µm
B
500 µm
C
500 µm
D
500 µm
E
1 mm
F
500 µm

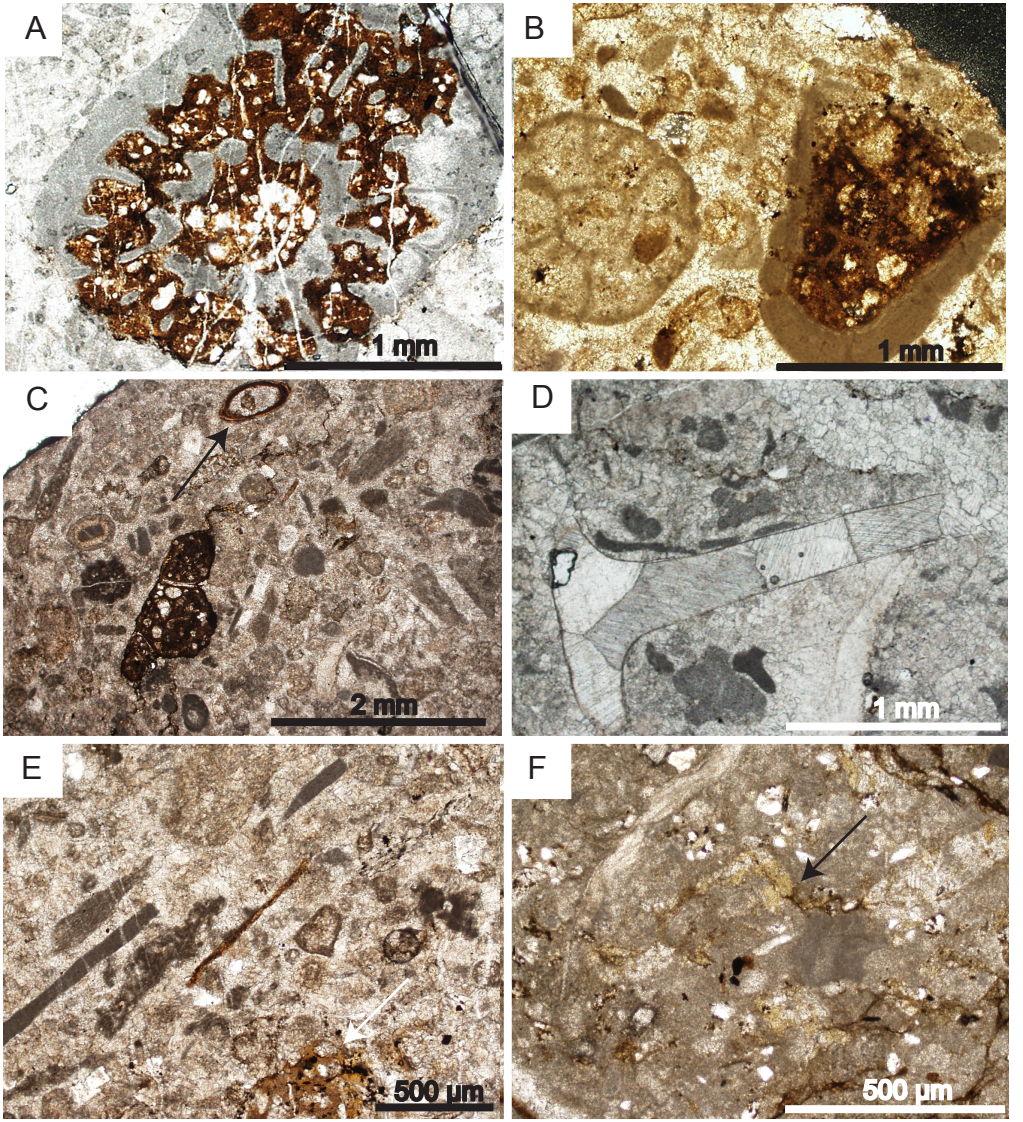
A
1 mm
B
1 mm
C
2 mm
D
1 mm
E
500 µm
F
500 µm

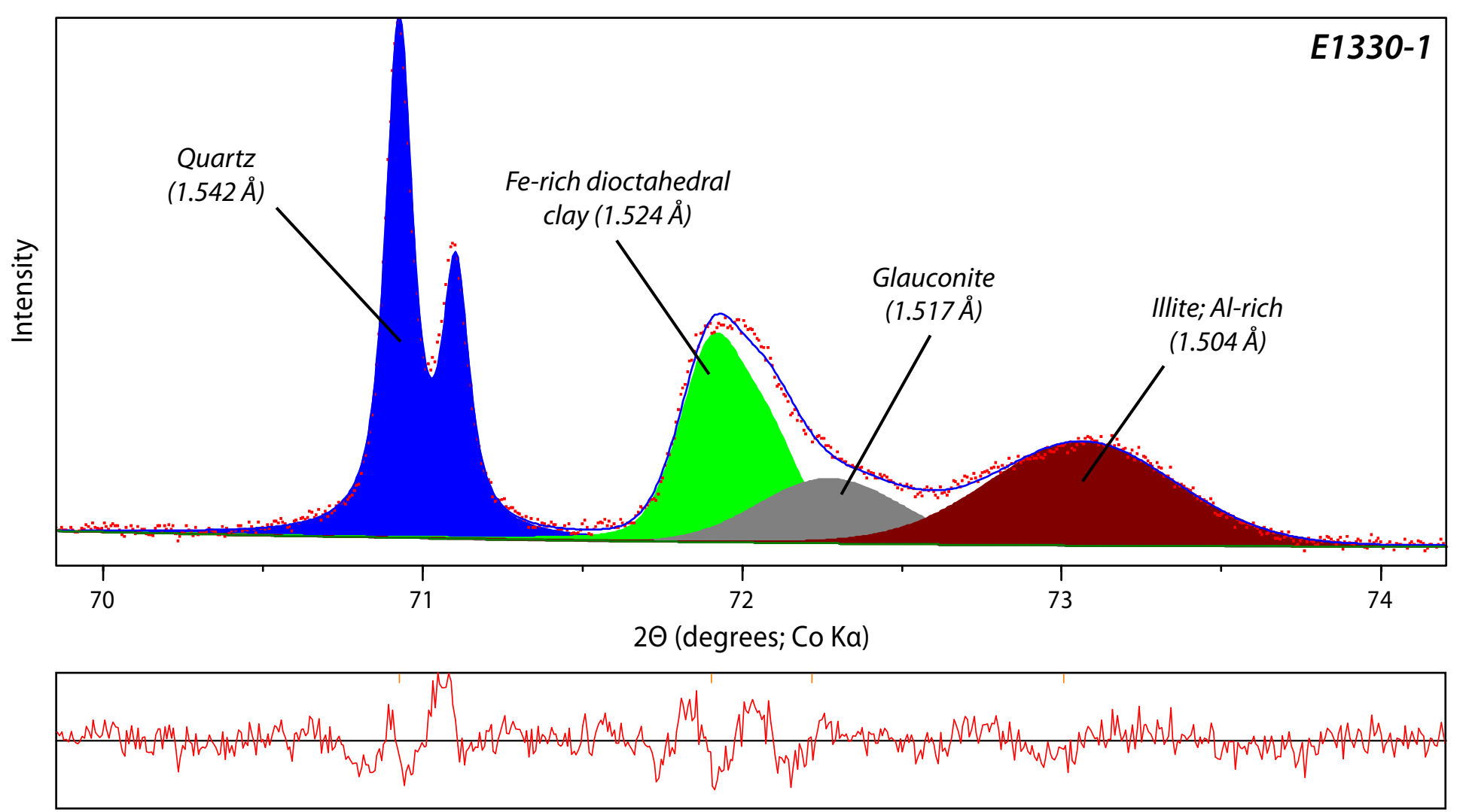
E1330-1
Quartz
(1.542 Å)
Fe-rich dioctahedral
clay (1.524 Å)
Glauconite
(1.517 Å)
Illite; Al-rich
(1.504 Å)
Intensity
70
71
72
73
74
2Θ (degrees; Co Kα)

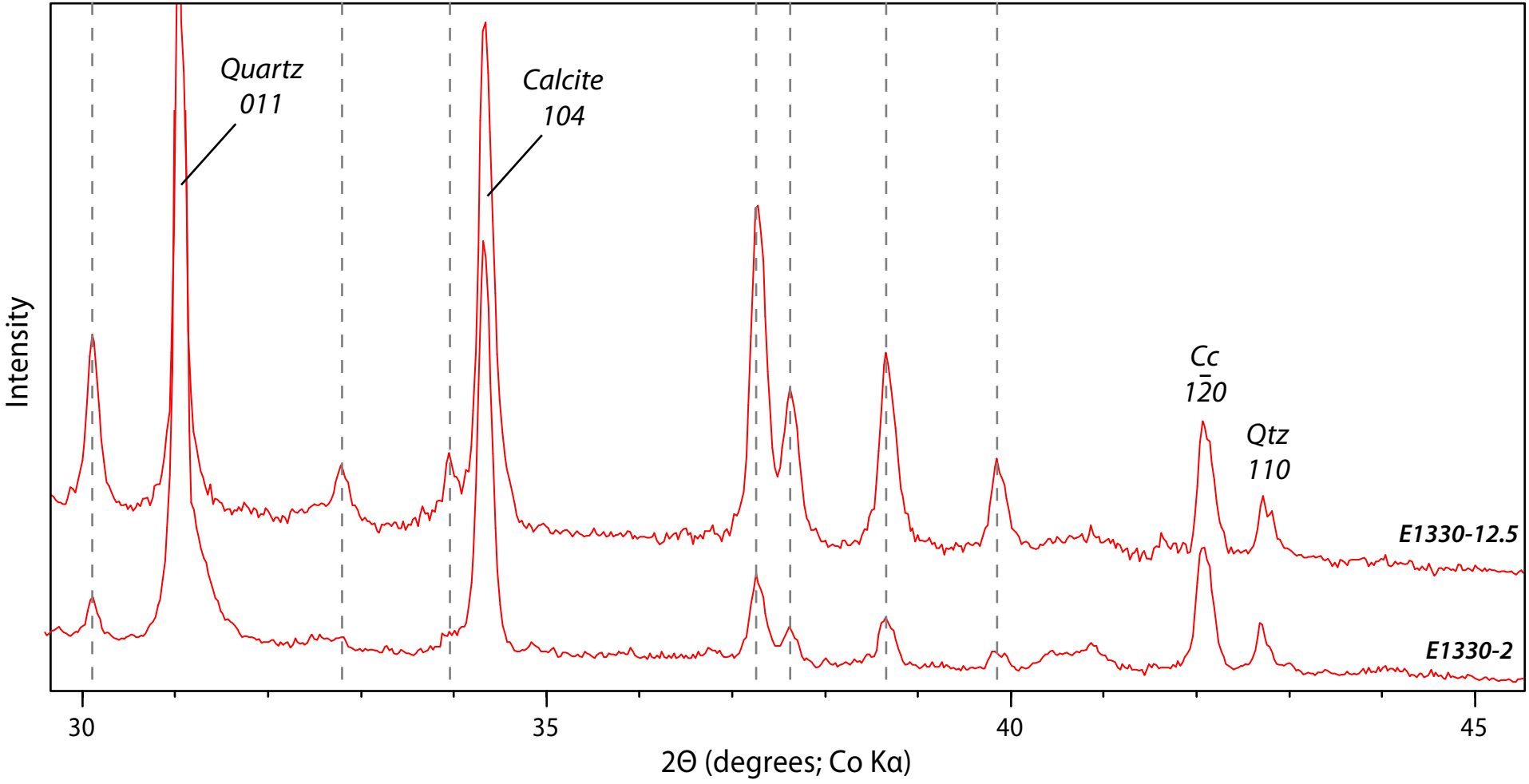
Quartz
011
Calcite
104
Cc
1$\bar{2}$0
Qtz
110
E1330-12.5
E1330-2
Intensity
30
35
40
45
2Θ (degrees; Co Kα)

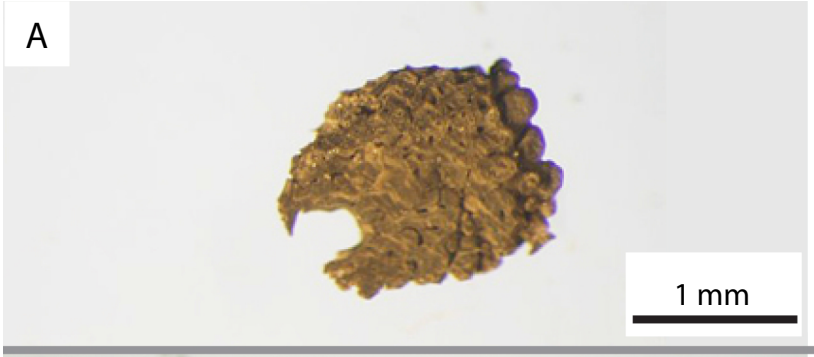
A
1 mm

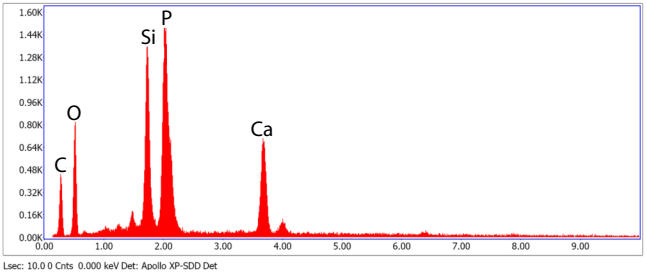
1.60K
1.44K
1.28K
1.12K
0.96K
0.80K
0.64K
0.48K
0.32K
0.16K
0.00K
C
O
Si
P
Ca
0.00
1.00
2.00
3.00
4.00
5.00
6.00
7.00
8.00
9.00
Lsec: 10.0 0 Cnts 0.000 keV Det: Apollo XP-SDD Det

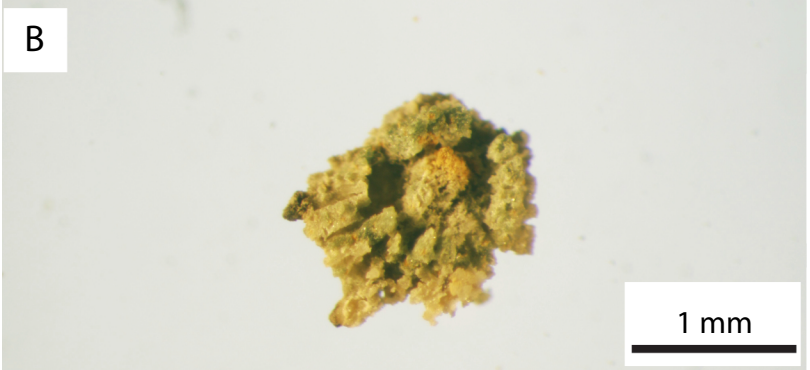
B
1 mm

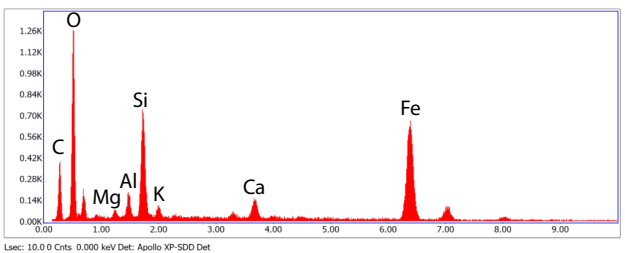
1.26K
1.12K
0.98K
0.84K
0.70K
0.56K
0.42K
0.28K
0.14K
0.00K
O
C
Si
Mg
Al
K
Ca
Fe
0.00
1.00
2.00
3.00
4.00
5.00
6.00
7.00
8.00
9.00
Lsec: 10.0 0 Cnts 0.000 keV Det: Apollo XP-SDD Det

A

Life position

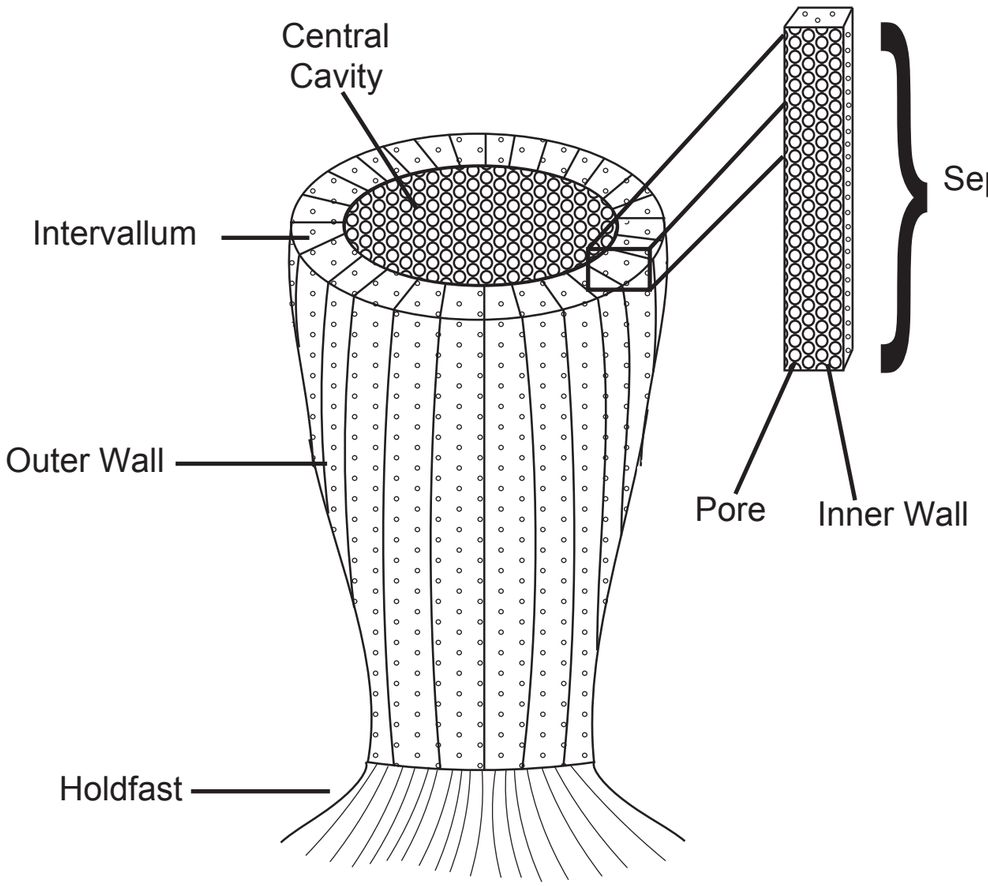


B

Transport

C

Preservation

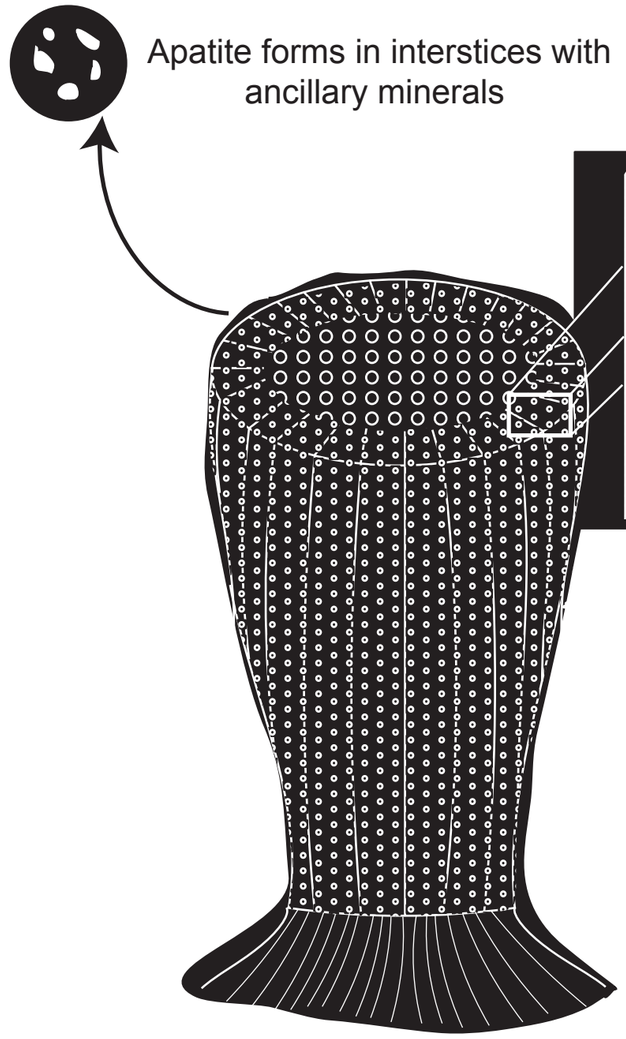

| Sample number | Sieve Size | Major Mineralogy | Minor Mineralogy | Major Skeletal Material | Minor Skeletal Material |
|---|---|---|---|---|---|
| E1221.1A1.20 | >840 µm | Phosphate | Quartz | Phosphatized archaeocyaths | |
| E1221.1A1.40 | 420-840 µm | Phosphate | Pyrite<br>Muscovite | Phosphatized archaeocyaths | Phosphatized chancelloriids |
| E1221.1A2.20 | >840 µm | Phosphate | Quartz | Phosphatized archaeocyaths | Phosphatized chancelloriids |
| E1221.1A2.40 | 420-840 µm | Phosphate | Muscovite | Phosphatized archaeocyaths | Phosphatized chancelloriids |
| E1221.2A1.20 | >840 µm | Phosphate | Quartz | Phosphatized archaeocyaths<br>Phosphatized chancelloriids | |
| E1221.2A1.40 | 420-840 µm | Phosphate | Pyrite<br>Muscovite | Phosphatized archaeocyaths | Phosphatized chancelloriids |
| E1221.2A2.20 | >840 µm | Phosphate | | Phosphatized archaeocyaths | Phosphatized SSFs |

| | | | | | |
|---|---|---|---|---|---|
| E1221.2A2.40 | 420-840 µm | Phosphate | Muscovite | Phosphatized archaeocyaths | Phosphatized and calcareous archaeocyaths<br>Calcareous archaeocyaths<br>Phosphatized chancelloriids<br>Phosphatized hyoliths |
| E1221.3A1.20 | >840 µm | Phosphate | Pyrite<br>Glauconite | Phosphatized archaeocyaths | Phosphatized chancelloriids |
| E1221.3A1.40 | 420-840 µm | Phosphate | Glauconite | Phosphatized archaeocyaths<br>Phosphatized hyoliths | Phosphatized chancelloriids |
| E1221.3A2.20 | >840 µm | Phosphate | Pyrite | Phosphatized archaeocyaths | Phosphatized and calcareous archaeocyaths<br>Phosphatized chancelloriids<br>Phosphatized hyoliths |
| E1221.3A2.40 | 420-840 µm | Phosphate | Pyrite<br>Glauconite | Phosphatized archaeocyaths<br>Phosphatized chancelloriids<br>Phosphatized hyoliths | |

| | | | | | |
|---|---|---|---|---|---|
| E1221.4A1.20 | >840 µm | Phosphate | | Phosphatized archaeocyaths<br>Phosphatized SSFs | |
| E1221.4A1.40 | 420-840 µm | Phosphate | Pyrite<br>Quartz | Phosphatized archaeocyaths<br>Phosphatized chancelloriids | |
| E1221.4A2.20 | >840 µm | Phosphate | Quartz<br>Muscovite | Phosphatized archaeocyaths<br>Phosphatized chancelloriids | Phosphatized and calcareous archaeocyaths<br>Calcareous archaeocyaths<br>Calcareous chancelloriids<br>Phosphatized hyoliths |
| E1221.4A2.40 | 420-840 µm | Phosphate | Quartz<br>Muscovite | Phosphatized archaeocyaths<br>Phosphatized chancelloriids | Calcareous archaeocyaths<br>Phosphatized hyoliths<br>Calcareous hyoliths |
| E1221.5A1.20 | >840 µm | Phosphate | Quartz<br>Glauconite | Phosphatized archaeocyaths | Calcareous archaeocyaths |
| E1221.5A1.40 | 420-840 µm | Phosphate | Glauconite | Phosphatized archaeocyaths | Phosphatized hyoliths |

| | | | | | |
|---|---|---|---|---|---|
| E1221.5A2.20 | >840 µm | Phosphate | Glauconite | Phosphatized archaeocyaths | Phosphatized and calcareous archaeocyaths<br>Calcareous chancelloriids<br>Phosphatized hyoliths |
| E1221.5A2.40 | 420-840 µm | Phosphate | Muscovite<br>Glauconite | Phosphatized chancelloriids | Phosphatized and calcareous archaeocyaths<br>Phosphatized archaeocyaths<br>Calcareous archaeocyaths<br>Phosphatized hyoliths |
| E1221.6A1.20 | >840 µm | Phosphate | Quartz | | |
| E1221.6A1.40 | 420-840 µm | Phosphate | Quartz<br>Muscovite | Phosphatized archaeocyaths<br>Phosphatized hyoliths | |
| E1221.6A2.20 | >840 µm | Phosphate | | Phosphatized archaeocyaths | |
| E1221.6A2.40 | 420-840 µm | Phosphate | Muscovite<br>Pyrite | Phosphatized chancelloriids<br>Phosphatized hyoliths | Phosphatized archaeocyaths |

| | | | | | |
|---|---|---|---|---|---|
| E1221.7A1.20 | >840 µm | Phosphate | Quartz<br>Muscovite<br>Glauconite | Phosphatized archaeocyaths | Phosphatized chancelloriids<br>Phosphatized hyoliths |
| E1221.7A1.40 | 420-840 µm | Phosphate | Quartz<br>Muscovite | Phosphatized archaeocyaths | Phosphatized chancelloriids |
| E1221.7A2.20 | >840 µm | Phosphate | | Phosphatized archaeocyaths | Calcareous archaeocyaths<br>Phosphatized chancelloriids<br>Phosphatized hyoliths |
| E1221.7A2.40 | 420-840 µm | Phosphate | | Phosphatized archaeocyaths | Phosphatized chancelloriids<br>Phosphatized hyoliths |
| E1221.8A1.20 | >840 µm | Phosphate | Quartz | Phosphatized archaeocyaths | |
| E1221.8A1.40 | 420-840 µm | Phosphate | Quartz<br>Muscovite<br>Glauconite | Phosphatized archaeocyaths<br>Phosphatized chancelloriids | Calcareous archaeocyaths<br>Phosphatized chancelloriids<br>Other Phosphatized SSFs |
| E1221.8A2.20 | >840 µm | Phosphate | | Phosphatized archaeocyaths | Phosphatized and calcareous archaeocyaths |

| | | | | |
|---|---|---|---|---|
| E1221.8A2.40 | 420-840 µm | Phosphate | Phosphatized chancelloriids | Phosphatized archaeocyaths |

| Sample Number | Majority Allochems | Minority Allochems | Majority Non carbonate grains | Minority Non carbonate grains | Size, Shape, Sorting of non-carbonate grains | Matrix |
|---|---|---|---|---|---|---|
| E1221.1A | Archaeocyaths<br>Peloids | Filamentous oncoids<br>Chancelloriids<br>Brachiopods<br>Hyoliths<br>Intraclasts | Quartz<br>Phosphate | Feldspar<br>Mica | Very fine;<br>Angular to subangular<br>Poorly sorted | Micrite<br>Recrystallized calcite<br>Phosphatic cement |
| E1221.2A | Archaeocyaths<br>Peloids | Chancelloriids<br>Brachiopods<br>Hyoliths<br>Intraclasts | Phosphate | | Very fine;<br>Unable to distinguish shape and sorting | Micrite<br>Recrystallized calcite<br>Vein of recrystallized calcite<br>Two styolites |
| E1221.3A | Archaeocyaths<br>Peloids<br>Intraclasts | Chancelloriids<br>Brachiopods<br>Hyoliths<br>Ooids | Phosphate | Quartz<br>Pyrite | Very fine;<br>Angular to subangular<br>Poorly sorted | Micrite<br>Phosphatic cement<br>Rounded phosphate grains<br>Styolite |
| E1221.4A | Archaeocyaths<br>Peloids | Chancelloriids<br>Brachiopods<br>Hyoliths<br>Filamentous oncoids<br>Ooids | Phosphate<br>Quartz | Glauconite | Very fine;<br>Unable to distinguish shape and sorting | Micrite<br>Phosphatic cement<br>Some styolites |

| | | | | | | |
|---|---|---|---|---|---|---|
| E1221.5A | Archaeocyaths<br>Peloids | Chancelloriids<br>Brachiopods<br>Hyoliths<br>Filamentous oncoids<br>Intraclasts | Phosphate<br>Quartz<br>Glauconite | Pyrite<br>Plagioclase feldspar | Very fine;<br>Angular to subangular<br>Poorly sorted | Micrite<br>Recrystallized calcite |
| E1221.6A | Archaeocyaths<br>Peloids | Chancelloriids<br>Brachiopods<br>Hyoliths<br>Intraclasts | Phosphate<br>Mica | | Very fine;<br>Unable to distinguish shape and sorting | Micrite<br>Recrystallized calcite<br>Phosphatic cement |
| E1221.7A | Peloids | Archaeocyaths<br>Chancelloriids<br>Brachiopods<br>Filamentous oncoids<br>Ooids | Phosphate<br>Quartz | Plagioclase feldspar | Very fine;<br>Angular to subangular<br>Poorly sorted | Micrite<br>Recrystallized calcite<br>Phosphatic cement |
| E1221.8A | Archaeocyaths<br>Peloids | Chancelloriids<br>Brachiopods<br>Hyoliths<br>Filamentous oncoids<br>Intraclasts | Phosphate<br>Quartz | | Very fine;<br>Angular to subangular<br>Poorly sorted | Micrite<br>Recrystallized calcite<br>Quartz vein<br>Styolites |

| Sample | Qtz | Fe-chl | Illite | Glau | Fe-clay | Apat | Sepio | Pyr | Plag | Total |
|---|---|---|---|---|---|---|---|---|---|---|
| E1330_0 | 68 | 4 | 11 | 5 | 12 | Tr | 0 | 0 | 0 | 100 |
| E1330_1 | 25 | 2 | 30 | 13 | 28 | 2 | 0 | 0 | 0 | 100 |
| E1330_2 | 26 | 5 | 29 | 8 | 26 | 5 | 0 | 0 | 0 | 100 |
| E1330_3 | 53 | 0 | 24 | 3 | 21 | 0 | 0 | 0 | 0 | 100 |
| E1330_5 | 77 | 0 | 10 | 3 | 8 | 0 | 3 | 0 | 0 | 100 |
| E1330_7 | 24 | 0 | 27 | 5 | 36 | 8 | 0 | 0 | 0 | 100 |
| E1330_9 | 72 | 0 | 18 | 6 | 5 | 0 | 0 | Tr | 0 | 100 |
| E1330_10 | 18 | 4 | 35 | 0 | 9 | 0 | 0 | 0 | 33 | 100 |
| E1330_11 | 21 | 3 | 27 | 0 | 18 | 0 | 0 | 0 | 31 | 100 |
| E1330_11.5 | 25 | 3 | 25 | 5 | 13 | Tr | 0 | 0 | 29 | 100 |
| E1330_12 | 28 | 9 | 12 | 2 | 9 | 3 | 0 | 0 | 36 | 100 |
| E1330_12.5 | 17 | 0 | 26 | 7 | 22 | 28 | 0 | 0 | 0 | 100 |